DEDUCING THE ROLE OF FUNCTIONALIZING MACROMOLECULES IN THE NUCLEATION OF COLLOIDAL NANOPARTICLES

by

Ece ALPASLAN

Submitted to the Graduate School of Engineering and Natural Sciences

in partial fulfillment ofthe requirements for the degree of

Master of Science

Sabanci University

July, 2013

DEDUCING THE ROLE OF FUNCTIONALIZING MACROMOLECULES IN THE NUCLEATION OF COLLOIDAL NANOPARTICLES

APPROVED BY:

Assoc. Prof. Cleva Ow-Yang
(Thesis Advisor) .....

Prof. Dr. Canan Atılgan .....

Assist. Prof. Alpay Taralp .....

Assist. Prof. Dr. Gözde İnce .....

Prof. Dr. Levent Demirel .....

DATE OF APPROVAL: 11/08/13

They always say an aunt is half of a mother. Mine has always been more than half.

To my beloved aunt

DEDUCING THE ROLE OF FUNCTIONALIZING MACROMOLECULES IN THE NUCLEATION OF COLLOIDAL NANOPARTICLES

Ece ALPASLAN

MAT, Master of Science Thesis, 2013

Thesis Supervisor: Assoc. Prof. Cleva Ow-Yang

Keywords: dynamic NMR, nanoparticle functionalization, macromolecule conformation

Abstract

Although polymers are widely employed to impart specific function to surfaces, techniques to characterize the adsorbed molecule are limited and usually indirect. We present two independent dynamic NMR studies to deduce the manner in which adsorbed poly-vinylpyrrolidone (PVP) attaches to the surface of ZnO colloidal nanoparticles and directs particle precipitation. In our colloidal system, the conformation of the polymer molecule on the particle surface—loosely described as trains, loops, or tails—can be elucidated by probing the nuclear response of the solvent or the polymer to pulsed magnetic fields. The dynamic ^{1}H-NMR signal of polymer-juxtaposed solvent molecules are monitored in our first approach, in which we monitor both spin-lattice (also known as T_1) and spin-spin (also known as T_2) relaxation behavior of the solvent, as the ease of solvent relaxation varies with proximity to the nanoparticle surface. In a second approach, the proton signal of the polymer is monitored over time. The rationale of this approach is that the signal of particle-bound polymer moieties will be lost faster than that of unbound polymer ones. Determining the signal of spin-echo and solid-echo processes enables calculation of polymer bound fraction.

The ZnO nanoparticle platforms are synthesized by the hydrolysis and condensation of zinc oxide precursors in PVP-containing solutions. Particle size distribution is determined by dynamic light scattering (DLS), as well as extrapolation from UV-visible absorption spectra.

Three specific PVP concentrations are chosen in producing ZnO particles. Synthesis in solutions of high PVP concentration produces comparable results between the hydrodynamic radius and the extrapolated UV-visible radius, whereas at low polymeric concentrations, the difference between the two radii increases, suggesting a change in the conformation of adsorbed polymer on the nanoparticle surface under varying concentration. Dynamic NMR T_1 analysis reveals a loss of solvent mobility at higher polymer concentrations.

In a separate experiment, we investigate the effect of the Zn precursor cations on the solvation of PVP, by using DLS to measure the hydrodynamic radius of the interpenetrating PVP in propanol, in the presence and absence of the zinc cation precursor. The results suggest that the zinc precursor ions pull the PVP chains closer, most likely due to the pyrrolidone rings on the polymers, and reduce the radius of gyration of polymer globules at high PVP concentrations. These results validate a model of highly dense polymer globules serving as reactors for ZnO nanoparticle precipitation, in which the high density of pyrrolidone rings in the globule hinders the diffusion of $Zn^{+2}$by electrostatic interaction. At high concentrations, large PVP globules appear to trap the reactant species and adsorb in a train conformation on the surface of precipitating ZnO nanoparticles. At low concentrations, the sizes of PVP globules are comparable to that of the evolving ZnO nanoparticles, and PVP adsorbs in looped and tail-only conformation.

FONKSİYONELLEŞTİRİCİ MAKROMOLEKÜLLERİN
KOLOİDE NANOPARÇACIK OLUŞUMUNDAKİ
ROLÜNÜN AYDINLATILMASI

Ece ALPASLAN

MAT, Master of Science Thesis, 2013

Tez Danışmanı: Doç. Dr. Cleva Ow-Yang

Anahtar kelimeler: dinamik NMR, nanoparçacık ile fonksiyonelleştirme, makromoleül konformasyonu

Özet

Polimerler yüzeylerin belirli fonksiyonlarını açığa çıkarmak için sıkça kullanıldıkları halde, yüzeye tutunmuş bu molekülleri karakterize etme teknikleri genellikle sınırlı ve dolaylı yollardandır.Poli-vinilpayrolidon (PVP) polimerinin koloidal ZnO nanoparçacıkları üzerine ne şekilde tutunduğunu anlayabilmek ve nanoparçacık oluşumuna nasıl katkı sağladığını anlamak için 2 ayrı dinamik NMR çalışması yapılabileceği tezini sunuyoruz. Koloidal sistemimizde, polimer molekülünün nanoparçacık üstündeki konformasyonu, polimer ya da solvent molekülünün uygulanan manyetik alana verdiği tepkiyi inceleyerek aydınlatabiliriz. Birinci yaklaşımımızda, polimer ile çevrilmiş solvent moleküllerinin ^{1}H ve ^{13}C dinamik NMR sonuçları takip edildi. Yüzeye yakınlıklarına bağlı olarak gevşeme hızları değişmesi beklenen solvent moleküllerinin hem T_1 (spin-kafes olarak da bilinen), hem de T_2 (spin-spin olarak da bilinen) gevşeme mekanizmaları analiz edilmiştir. Ikinci yaklaşımımızda ise, polimerden gelen proton sinyalinin zamanla değişimi incelenmiştir.Bu yaklaşımın arkasındaki fikir,

parçacığa bağlı olan kısımlardan gelen sinyallerin bağlı olmayan yerlerden gelen sinyallerden daha hızlı kaybolacağıdır.Spin- eko ve katı-eko sürecinin çözümlenmesi parçacık yüzeyine bağlı polimer yüzdesini hesaplayabilmemizi mümkün kılacaktır.

ZnO nanoparçacıkları, çinko oksit öncü maddesinin PVP içeren solüsyonlarda hidroliz ve yoğunlaşmasıyla elde edilir.Parçacık boyu dağılımı, dinamik ışık saçılımı (DLS) ve UV-görünür bölge spektroskopisinin ekstrapolasyonu ile elde edilmiştir.ZnO nanoparçacıklarını sentezlemek için 3 ayrı PVP konsantrasyonu seçilmiştir. Yoğun PVP konsantrasyonlarında sentezlenen parçacıkların hidrodinamik yarıçapı ve UV-görünür bölge spektroskopisinden elde edilen yarı çapı yakın değerlerdeyken, düşük polimer konsantrasyonlarında 2 değer arasındaki fark artmaktadır

Ayrı bir deney setinde, çinko öncü madde katyonlarının PVP'de çözünmesinin parçacık boyutuna olan etkisini iceledik.1-propaol'de çözünmüş ve içiçe geçmiş polimer zincirlerinin Zn öncü maddesi iyonu olan ve olmayan ortamda hidrodinamik yarıçapını, DLS'de ölçerek elde ettik.Sonuçlara göre, yüksek polimer konsantrasyonlarında Zn öncü maddesi iyonları, büyük olasılıkla payrolidon halkasından ötürü PVP zincirlerini birbirlerine yakınlaştırıyor ve atalet yarıçapını (R_g) düşürüyor.Bu sonuçlar, polimer konstrasyonunun yüksek olduğu durumlarda, polimer moleküllerinin ZnO nanoparçacık oluşumunda reactor görevi gördüğünü doğruluyor.Payrolidon halkasının konsantrasyonunun yüksek olması, elektrostatik etkileşimler ile Zn^{+2} iyonunun difüzyonunu engelliyor.Yüksek konsantrasyonlarda PVP globülleri reactant maddeleri içine hapsederek, ZnO nanoparçacık oluşurken polimerlerin tren konformasyonunda yüzeye tutunmasını sağlıyor.Düşük polimer konsantrasyonlarında ise 1-propanolde çözünmüş PVP zincirleri içiçe geçmek yerine, tek tek zincirler halinde stabil kalıyorlar ve Zn^{+2} li ortamda birbirlerine daha çok yaklaşarak bir globül oluşturuyorlar.PVP yüzeye daha çok tek bir yerden bağlanıyor ya da halka şeklinde konformasyonalar oluşturuyor.

Table of Contents

LIST OF FIGURES:

LIST OF TABLES:

ACKNOWLEDGEMENTS

My most humble and sincere thanks to:

As always, first and forements, to my advisor, Cleva Ow-Yang for her guidance, wisdom, patience, support, motivation and friendliness that she shared with me through out my master studies. Apart from trying to help me to build a strong theoretical background, she made me remain undettered by diffuculty.

Canan Atılgan and Alpay Taralp for showing an incredible amount of interest to my work on macromolecules and Nuclear Magnetic Resonance. I have learned a lot from them during both my graduate and undergraduate years in Sabanci Univeristy.

Gözde İnce and Levent Demirel for agreeing to attend my dissertation and for their valuable comments on my thesis.

Burçin Yıldız, for her help with the Nuclear Magnetic Resonance experiments.

Hasan Kurt and Güliz İnan not only for their help in my experiments and characterizations, but also for their friendliness, enthusiasm, creativity and efforts on behalf on my thesis work.

My office mates, Mustafa Baysal, Melike Mercan Yıldızhan, Senem Avaz, Pelin Güven and Canhan Şen for being great office mates and cheering me up.

Whole MAT group for their friendliness, for not hesitating sharing their expertise

My parents Bayram Alpaslan and Aynur Alpaslan for their unending support, and love.

My aunt Ayfer Sarıgül, for being always there for me, supporting me, loving me.

My life is in Sabanci University is not limitted to just last two years. I would also like to thank to dear friends who made my life a lot more bearable in Sabanci University in my undergraduate years. Many thanks to Hakan Sadıkoğlu, Simin Fadıllıoğlu, Asaf Nisan Güler, Kübra Kandemir, Emre Kılıçel, Gonca Ceylan and Emir İzmiroğlu.

My boy friend Mehmet Ali Güney, for his unending love, making my life a lot more easier and for the inspiration that he gave me.

My great great sister Elif Alpaslan for believing in me no matter what, and supporting me in every decision I have made. I am eternally grateful

1 Introduction

1.1 Polymer-functionalized nanoparticles

Precipitation of ZnO colloids can be explained with the formation and growth of wurtzite crystals. The properties of those particles can be determined by the unpaired electrons at the surface. To have a better control on those unpaired electrons and stabilize them,polymer macromolecules and ligands are used during the synthesis of colloidal nanoparticles to prevent aggregation [1,2]. Generally, dispersion of nanoparticles within a polymeric environment has proven to be difficult and mostly results in phase separation and agglomeration. For example, in the case of ZnO nanoparticles, which have attractive UV luminescence properties, the adsorption of poly-(vinylpyrrolidone) (PVP) enables the engineering of colloids with desirable surface characteristics, while maintaining the optical behavior [3]. This ability to engineer interfacial properties has opened up a variety of important applications for nano-scale colloids, such as in nanocomposites and in drug delivery.

1.1.1 Nanocomposites

Nanocomposites are advanced materials offering technologically attractive mechanical, optical, thermal, and electrical properties unattainable by their individual constituent materials alone or with fillers on the micron-size scale. Nanoscale materials have high surface to volume ratio. Since surfaces govern many important physical and chemical interactions, a nanostructured material can have very different properties than a larger dimensional material of the same composition [4-7]. The properties of nanocomposites are greatly affected by degree of mixing between two phases and size scale of the component phase. The research on nanocomposites is extremely broad including the following areas: Electronics, computing, data storage, communications, aerospace and sporting materials, health and medicine, energy, environmental transportation and national defense applications [4].

A polymer nanocomposite consists of a nano-sized scale filler with at least one dimension less than 100nm well-dispersed within a polymer matrix [8].A good dispersion and adhesion of nanosized material at the particle matrix interface play a crucial role in determining the mechanical properties. Unless the good dispersion is achieved, nanomaterial will not offer an improved mechanical property. In fact, poor dispersion of nanomaterial may deteriorate the mechanical properties. A good adhesion at the interface will contribute the enhancement of interlaminar shear strength, delamination resistance, fatigue and corrosion resistance [9]. With the addition of carbon nanotubes and graphite particles, an increase in the conductivity of the polymer was observed [4, 10]. Compared to any micro or macrocomposites and bare polymers, nanocomposites have much less gas permeability as well as flammability [11, 12]. A high aspect ratio (i.e. plate-like) in filler particles does have an effect on how particles are dispersed in the nanocomposite, which is a key parameter for determining the properties of the overall composite [8,11].

1.1.2 Drug Delivery

Another important application of polymer/nanoparticle systems are drug delivery applications. Nanoparticles are attractive candidates for drug delivery, because they have the ability to deliver a wide range of drugs to targeted areas of the body. One drawback of sending a drug-loaded, bare nanoparticle into body is their rapid clearance by "phagocytosis"[13]. To solve this problem, recently carrier particles, which are to be loaded with drugs, have been functionalized with macromolecules. The macromolecules serve as an "invisibility cloak" for the nanoparticle. Natural polymers like proteins and polysaccharides lack purity. So, synthetic polymers have attracted great attention in this manner. There are fourmain parameters that control the efficiency of the drug carriers in polymer functionalized nanoparticle systems: Size of the particles, encapsulation efficiency of the particle, zeta potential and release characteristics [13].

1.2 Precipitation of ZnO colloids

There are many possible routes for synthesis of ZnO nanoparticles. Sol-gel technique is the most preferred one since it does not require elevated temperatures [14-17].The general procedure is hydrolyzing zinc salts which are dissolved in the alcohol with a with a strong basic oxygen source like NaOH, KOH or LiOH. And this step is followed by precipitation of $Zn(OH)_2$as particles.

1.3 The Physical Properties of Polymers in Solution

1.3.1 Polymer Interaction with Solvent

The chain dimensions of amacromolecule in solution depends on thethe solvent-molecule interactions. A solvent can be a poor, theta (θ) or good solvent with respect to its interaction

with the polymer. If the affinity between the solvent and the polymer beads is high, the solvent is called as good solvent. And the macromolecules will be more extended in the solvent owing to excluded volume interactions between monomer beads. The other extreme would be when the polymer does not dissolve well in the solvent. This type of solvent is called as a poor solvent. The polymer chain will be shrunken or collapsed within the solution, minimizing contact with the solvent molecules. A special intermediate case would be a theta solvent,in which the macromolecule segmentsbehavelike ideal chains (*i.e.* no intramolecule interactions). The excess chemical potential of mixing between a polymer and a θ solvent in this situation is zero, due to the compensation of repulsive excluded volume interactions and monomer-monomer attractive interactions. [18,19].

1.3.2 Conformations of Ideal PolymerChains

In order to understand the possible conformations for a polymer chain, the distance between the neighboring atoms, the angle between the neighboring bonds, *i.e.*the *tetrahedral bond angle* θ, and the torsion (*i.e.* rotation) angles $\psi_i$needs to be considered which are shown in Figure 1.

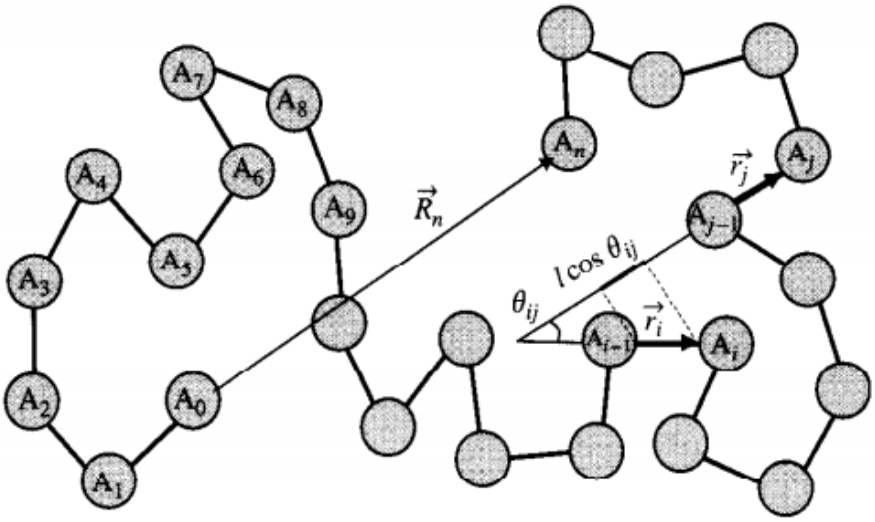

Figure 1: **One possible polymer conformation illustrating the characteristic parameters of the polymerchain. Adapted from reference 18.**

There are several models in order to explain the size and characteristics of the polymers, making different assumptions on allowed values of torsion and bond angles. The conformation of an ideal chain, where it is assumed to have no interaction between the polymer beads, is essential starting model of most models in polymer physics [20].

The simplest model for an ideal polymer chain is the *freely jointed chain model*, where there is a constant bond length of $l = 1\vec{r}_i$ land no correlations between the directions of the different bond vectors.

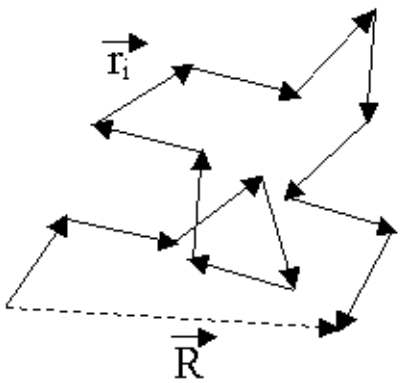

Figure 2: Representation of random walk. Adapted from reference 18.

When a freely jointed linear polymer with *N* sub-units and each of the sub-unit has a bond length of *l*, the volume of each unit is neglected, so that no part of the chain excludes another part from any location, this kind of chain performs random walk (Fig.2). This is the ideal chain mathematical model. The coil dimensions are characterized by root-mean-square (rms) end-to-end distance. For a freely jointed chain rms value can be calculated by:

$$\langle R^2 \rangle = nl^2 \qquad \text{(Eqn. 1)}$$

Another model for ideal chains is *freely rotating chain model*. In freely rotating chain model, the difference between probabilities of different torsion angles is ignored (Fig.3). It assumes all torsion angles are equally probable and all bonds lengths and bond angles are assumed to be fixed.

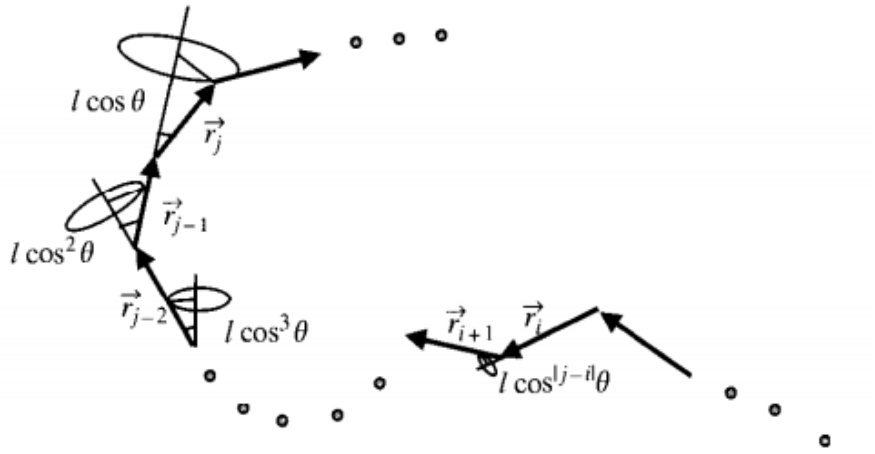

Figure 3: In freely rotating chain model all torsional angles are equally probable. Adapted from reference 18.

PVP is linear, non-ionic polymer. It has high polarity and it is soluble in any polar solvent. Water and alcohols (*i.e.* propanol, isopropanol) act as good solvents for PVP[21]. At low polymer concentrations, for PVP dissolved in propanol freely rotating chain model can be applied.

The mean square end-to-end distance for the freely rotating chain model can be calculated with the equation below:

$$\langle R^2 \rangle = nl^2 + l^2 \sum_{i-1}^{n} \left(\sum_{k=1}^{i-1} \cos^k \theta + \sum_{k=1}^{n-i} \cos^k \theta \right) \quad \text{(Eqn.2)}$$

1.3.3 Overlap Concentration

Polymer solutions can be classified according to their concentrations asdilute and semi-dilute concentrations.Concentration can be described by the volume fraction,ϕ, the ratio of occupied volume of polymer in the solution to volume of solution [18].

$$\phi = c \frac{V_{mon} N_{AV}}{M_{mon}} \quad \text{(Eqn.3)}$$

The pervaded volume V is defined as the volume of solution that is spanned by the polymer chain. The volume fraction of a single molecule inside its pervaded volume is called the *overlap volume fraction* ϕ^*.

$$\phi^* = \frac{N V_{mon}}{V} \quad \text{(Eqn. 4)}$$

The polymer solution is filled with the pervaded volumes of polymer and chains are about to overlap, when the volume fraction ϕ of the polymer solution is equal to overlap volume fraction ϕ^*($\phi=\phi^*$).

When polymer volume fraction $\phi$is less than the overlap volume fraction ϕ^*(*i.e.*, $\phi<\phi^*$), the solution is considered to be dilute. In dilute solutions the size of each polymer chain is less than the average distance between the chains. So the chains in dilute solutions are well separatedand solvated.

If the volume fraction is above the overlap volume fraction, the solution is considered to besemi-dilute (*i.e.*, $\phi>\phi^*$). Polymer chains overlap and interpenetrate. In these systems most of the physical properties, such as viscosity, are dominated by the dissolved polymer.

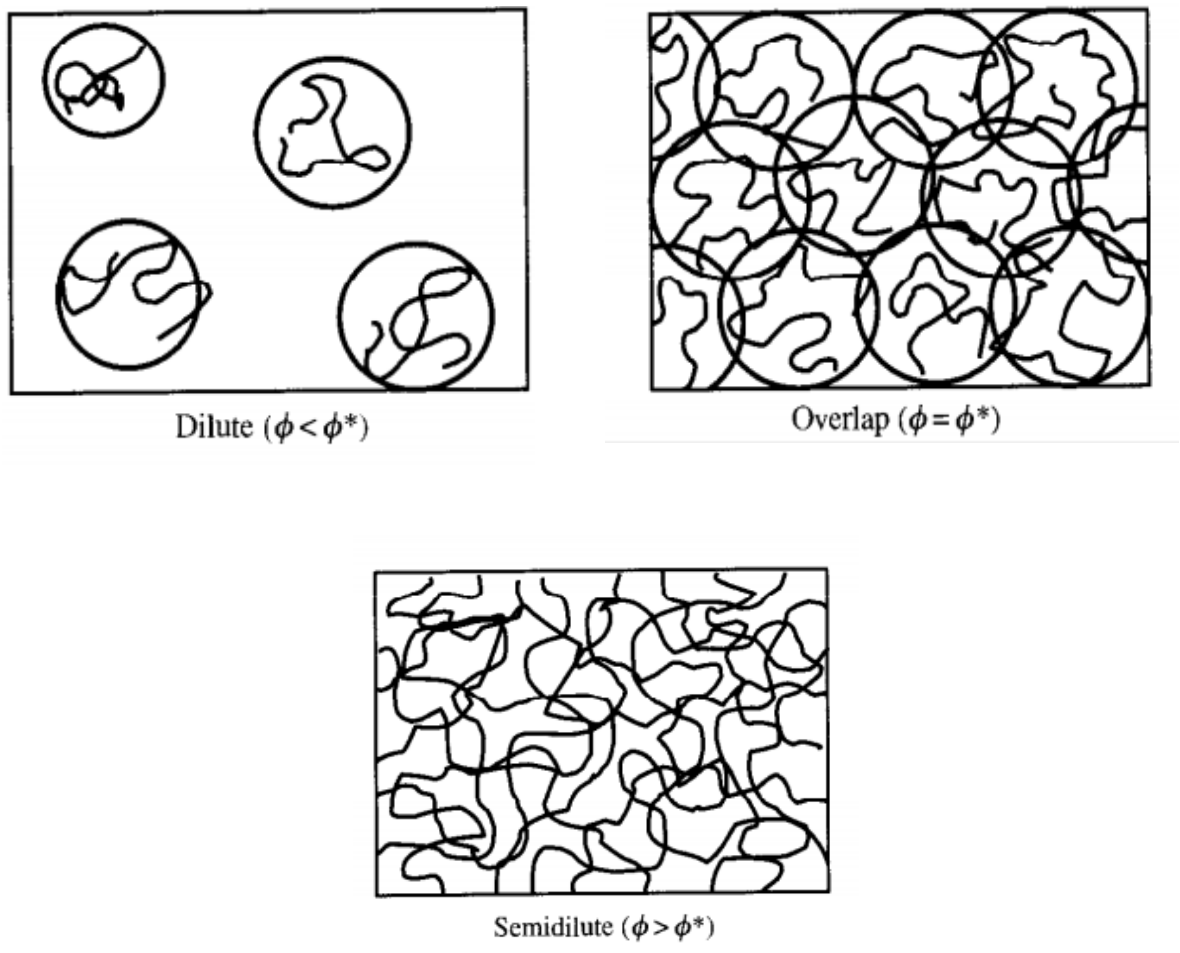

Figure 4: Representation of solutions with different polymer concentrations. Adapted from Reference 18.

1.3.4 Hydrodynamic Radius

The hydrodynamic radius (R_H) is the apparent radius of particle or macromolecule in solution, including solvent molecules that may be clustered around the particle. A common way for measuring the hydrodynamic radius is through Dynamic Light Scattering (DLS). The basic idea behind DLS is that light is scattered by particles suspended in solution. Particles in suspension are constantly moving due to the thermal fluctuations, also known as "Brownian motion."The degree of Brownian motion depends on particle size and density, viscosity of solution, and temperature [22]. The diffusion coefficient, D, of a spherical particle with R_H, in a solution with viscosity η, at a temperature T with is estimated through the Stokes-Einstein relation in Equation 5.

$$D = \frac{kT}{6\pi\eta R_H} \qquad \text{(Eqn.5)}$$

where$k$ is the Boltzmann constant. Light scattering will change from one time instant to the next as the particles move. By monitoring the relative degree of change in the scattered pattern over time, i.e. the *correlation* of the scatter pattern, we can deduce D and thus estimate R_{H}. For example, a large particle would move more slowly than a smaller version of the same material. Thus the correlation between scattered patterns would be maintained over a longer length of time. By contrast, a smaller particle would be more mobile, and the correlation between light scattered patterns would be lost more quickly.

1.3.5 Radius of Gyration

The radius of gyration, R_g, is a commonly used measure of size for solvated macromolecules or macromolecules in the melt state. It can be defined as the average distance of every single bead to centre of gravity [23] (Figure 5). Mathematically it can be denoted as in Equation 6.

$$< s^2 >= \frac{1}{N+1} < \sum_{i=0}^{N} (R_i - R_c)^2 > \qquad \text{(Eqn. 6)}$$

Where R_i is the coordinate position for i^{th} bead, R_c is the center of gravity, N is the *chain length*, (N+1) is the number of beads in a chain of length N.

Figure 5: Schematic of the difference between hydrodynamic radius and radius of gyration.

The radius of gyration is not a directly measurable value, whereas hydrodynamic radius is. However, for spherical particles, there is a theoretical constant between them [24]:

$$\frac{R_g}{R_h} \sim 0.77 \qquad \text{(Eqn.7)}$$

Here in this thesis, R_g is used to define the radius of the polymer globule which is composed of many chain's entanglement (i.e. overlap) within the solution. Basically it is the average distance of each mer of the chains in the globule from the gravitational center of the globule (Fig.5).

1.4 Light Scattering

It is known that all media, even solvent molecules scatter light. A macroscopically homogenous media scatter light due to *density fluctuations*. We can therefore leverage the manner in which light is scattered to extrapolate structural characteristics of polymeric solutions.

When polymer molecules are dissolved within a solution, this scattering occurs due to the *polymer concentration fluctuations*. This phenomenon is called *excess scattering* and it is used in order to investigate on the properties of polymers [25].

1.4.1 Rayleigh Light Scattering in Dilute Polymer Solutions

In Rayleigh Light Scattering model, it is assumed that there is no change in the frequency of the scattered light. If it is assumed that the incident beam of light has wavelength of $\lambda_0$and an intensity of J_0 it passes through a dilute polymer solution a detector at a distance r measures the intensity of excess scattering J as a function of scattering angle θ.

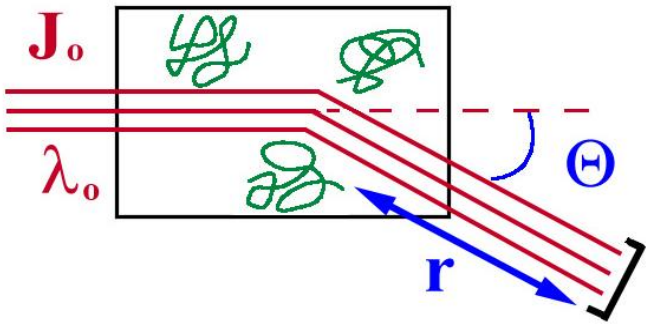

Figure 6: Light scattering in dilute polymer solutions. Adapted from reference 25.

Polarizibility has an influence on the intensity on the intensity of the scattered light and molecular weight has an influence on the polarizability. Besides the molecular weight dependence, light scattering has also dependent on the particle size. For polymer solutions this dependence on size can be used to measure the radius of gyration of polymer molecule. Rayleigh theory is applicable for small particles whose size is smaller than the wavelength of the scattered light, as summarized by following relation:

$$\sqrt{< R_g^{\,2} >} < \frac{\lambda}{20} \qquad \text{(Eqn.8)}$$

Since the wavelengths of visible light fall between 400-800 nm, a physically meaningful root mean square radius of gyration should liebetween 20 to 40 nm [26]. Most of dissolved polymer chains may not possess an $R_g$occuring this region, so they cannot be treated as point scatterers. In this case, the destructive interference of light scattered by different monomer units should be taken into account.

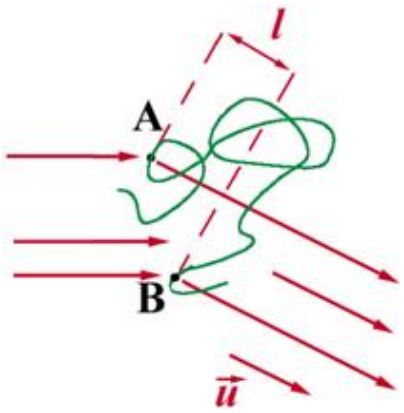

Figure 7: Light scattering of polymers with larger sizes. Adapted from reference 25.

In figure7, light waves scattered from the monomer units ***A*** and ***B*** in the direction of the unit vector $\hat{u}$ are shifted in phase with respect to each other, because of the excess distance ***l.*** This phase shift is small, as soon as $l << \lambda$**,** but still it is responsible for the partially destructive interference which leads to the decrease in *I.* This effect should be larger for higher values of scattering angle, θ.

By measuring the angular dependence of scattered light it is possible to obtain the mean square radius of gyration of a polymer chain $\langle R_g^2 \rangle$.

1.5 Interfacial Engineering with Polymers

The scope of this thesis is restricted to a model polymer macromolecule poly-vinylpyrrolidone (PVP), which is a linear polymer and a polyelectrolyte. Polyelectrolytes are macromolecules whose repeating units bear an electrolyte group. Thus, physical properties of this molecule are dominated by electrostatic interactions [27]. In Figure 8, chemical structure of vinylpyrolidone mer is shown.

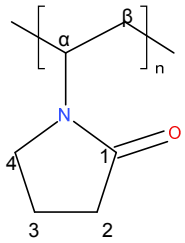

Figure 8: The chemical structure of vinylpyrrolidone mer. *n* corresponds to the number of repeating units

This mer contains a carbonyl group, which coordinates strongly with Zn cations [28]. Thus, PVP is commonly used to functionalize colloidal ZnO particles.

The physical behavior of a linear macromolecule like PVP is determined by its molecular weight, i.e. the number of repeat units *N*(Figure 9) and its apparent size when solvated—the hydrodynamic radius and the radius of gyration.

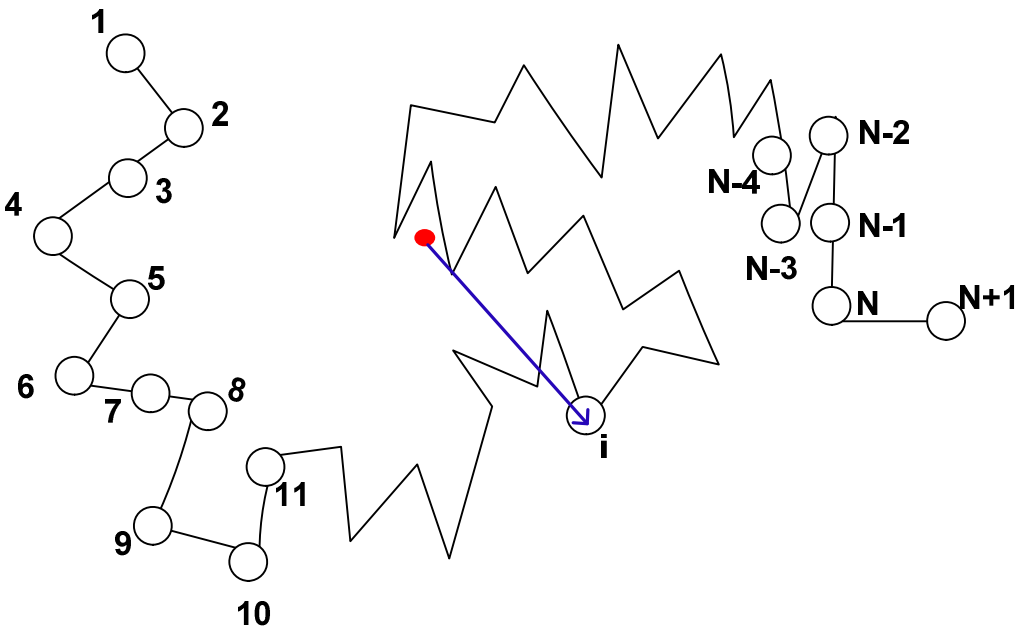

Figure 9: Polymer chain with *N+1* repeating units and *N* bonds.

1.6 Polymer Conformation

Because the manner in which a polymer is adsorbed on a colloidal nanoparticle surface can permit or evade cell uptake in drug delivery applications [29] and dictate nanocomposite mechanical properties (*viz.* elastic modulus, strength, and glass transition temperature) through the interparticle distance engendered, [30-37] macromolecule conformation is thus an important parameter for engineering polymer-functionalized nanoparticles.

Potential applications listed above establish the need to control the interface formed between the polymer chains and the nanoparticle surface. Not all the segments of polymer chains are adsorbing onto the surface of nanoparticles. There are three possible conformations for a polymer to be adsorbed onto the surface: train, loop or tail conformation. If all of the segments are present at the surface, it is called train conformation. If only both ends of the polymer chain attach to surface, it is a loop conformation (Figure10). Lastly, in tail conformation polymer adsorbs from its one end and rest of the chain is well solvated into the solution [38].

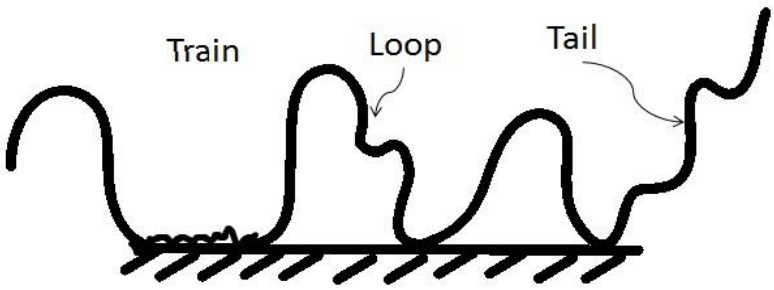

Figure 10: Possible polymer conformations at the interface

1.7 NMR

Nuclear magnetic resonance (NMR) spectroscopy is a unique and powerful characterization technique for determining polymer properties in both the solution and the solid state. The reason why is, many molecular level features can be measured from NMR spectra, including polymer microstructure, chain conformation and dynamics of the system[39]. To date, numerous techniques have been developed to determine the manner by which a macromolecule adsorbs onto a surface, including ESR, NMR, IR, neutron scattering [40].Solution-state NMR in particular offers highly accurate qualitative and quantitative information about chemical structure through the use of magnetic resonance and response to analyze physical and chemical properties. It enables analysis of the interaction of a collection of nuclei immersed in a strong, static magnetic field, when exposed to a second oscillating magnetic field [41].

In 1902 the Dutch physicist P. Zeeman shared a Nobel Prize for his discoveries on the nuclei of some atoms behaving strangely, when they are exposed to an external magnetic field. Around 50 years later, two physicists F. Bloch and E. Purcell shared another Nobel Prize for making this so-called nuclear Zeeman Effect to practically usable by building the first crude NMR spectrometer [41].

As Zeeman discovered in 1902,some nuclei experience this phenomenon, while others cannot. The reason why the NMR phenomenon is possible for some nuclei is attributed to their spin properties, which respond to magnetization. If the proton within a nucleus possesses spin, then that molecule can be called NMR-active. In an NMR experiment, spins of nuclei are exposed to a magnetic field and the net magnetization of spins is observed by disturbing the system with an oscillating magnetic field. Spins can either align with or against the magnetic field. Physical meaning of a spin can be associated with angular momentum and a tiny

magnetic field called magnetic moment associated with this angular momentum. For a nucleus possessing a spin the maximum experimentally observable component of the angular momentum is half integral or integral multiple of $h/2\pi$, where h is the Planck's constant [39]. This maximum component is called spin quantum number or 'the spin', which is denoted by I. The magnitude of the nuclear magnetic moment (μ), depends on the ratio of the magnetic moment to the angular momentum. That parameter is called magnetogyric ratio (γ), and it is given by Equation 9,

$$\gamma = \frac{2\pi\mu}{Ih} \qquad \text{(Eqn.9)}$$

Spins are quantized, meaning that only discrete spins are allowed. However, not all the nuclei possess spin. The spin quantum number tells us whether or not the nuclei possess spin. Table 1 lists the spin properties with respect to nuclei properties.

Table 1: Spin quantum number with respect to proton and neutron number in the nuclei

Spin	**Number of Protons and Neutrons**	**Spin Quantum Number**
Integral Spin	Even mass nuclei: odd number of protons and neutrons	$I = 1$ (^{2}H, ^{14}N)
Fractional Spin	Odd mass nuclei: odd number of nucleons	$I = 1/2$ (^{1}H, ^{13}C, ^{19}F) $I = 3/2$ (^{11}B) $I = 5/2$ (^{17}O)
No Spin	Even mass nuclei: even numbers of protons and neutrons	$I = 0$ (^{12}C, ^{16}O)

Generally, there are *2I*+1 available states or orientations of nucleus. For instance, if the spin quantum number is ½, the possible quantum numbers are ½ and – ½, indicating that either spins are aligned with or against to applied magnetic field. Figure 11, shows energy diagram for spin quantum number ½ and 1

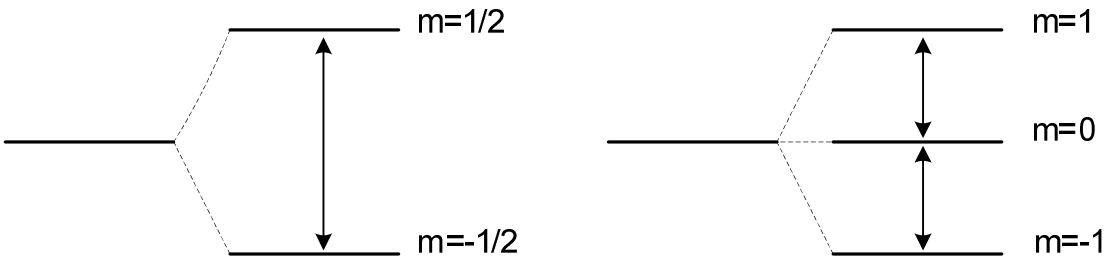

Figure 11: Energy level diagram for I=1/2 and I = 1 spin systems.

Nuclear spin undergoes precession to return to its equilibrium state, when exposed to a magnetic field, as shown in Figure 12. The frequency of this precession is called Larmor frequency, which is denoted by ω_o in units of radians per second or v_o in herts (Hz), cycles per second. The Larmor precession frequency is given by Equation 10.

$$\omega_0 = \gamma B_0 \qquad \text{(Eqn.10)}$$

whereB_0 is the strength of the applied magnetic field.

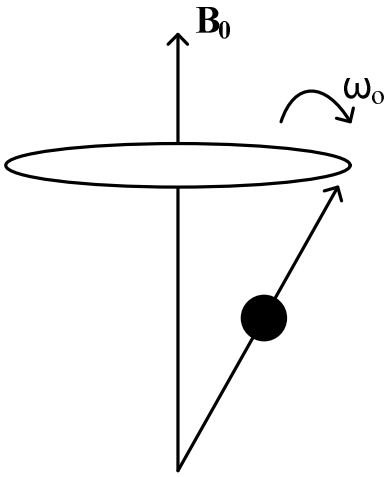

Figure 12: Precession of a magnetic moment under applied magnetic field

To be able to obtain a good NMR signal (*i.e*. high signal to noise ratio) magnetogyric ratio and the natural abundance of the NMR active nuclei is important. For example, in proton NMR the signal-to-noise ratio is low, because hydrogen's magnetogyric ratio is low, and its natural abundance is around 100%. However, for detecting ^{13}C, which is a very common element for polymers, we need to wait longer, since its natural abundance is low. Table 2summarizes some of the properties of the NMR-active nuclei.

Table 2: The NMR Properties of Nuclei of Interest to NMR Spectroscopists

Isotope	Abundance (%)	Spin	$\gamma^* 10^{-8}$	Relative Sensitivity	$v_o$at 11.7 T (MHz)
^{1}H	99.98	½	2.6752	1.0	500.
^{19}F	100.	½	2.5167	0.83	470.2
^{29}Si	4.7	½	-0.5316	0.078	99.3
^{31}P	100.	½	1.0829	0.066	202.3

^{13}C	1.1	½	0.6726	0.0159	125.6
^{2}H	0.015	1	0.4107	0.00964	76.7
^{15}N	0.365	½	-0.2711	0.0010	50.6

The quality of the acquired data depends on several parameters: Sample preparation techniques, the spectrometer, choosen NMR experiment, the NMR parameters and the methods which are used for acquiring the data.

Different spin populations are observed due to the energy splitting under magnetic field. Using the Boltzman distribution, we can determine the population of upper and lower spin states. Spins can align with (the α state) or opposing (the β state) the applied magnetic field. The population in the upper spin state (N^+) and the lower spin state (N^-) are determined by Equation 11.

$$\frac{N^+}{N^-} = 1 + \frac{2\pi\mu}{kT} \qquad \text{(Eqn. 11)}$$

In an NMR experiment, the nuclei of atoms (*i.e.* spins) are exposed to magnetic field. In Figure 13a, the equilibrium state of immersed spins is shown. According to Boltzmann distribution, the spin population is higher at one of these states. In Figure 13b, a single vector is shown representing the sum of all spin vectors in the system, and called net magnetization.

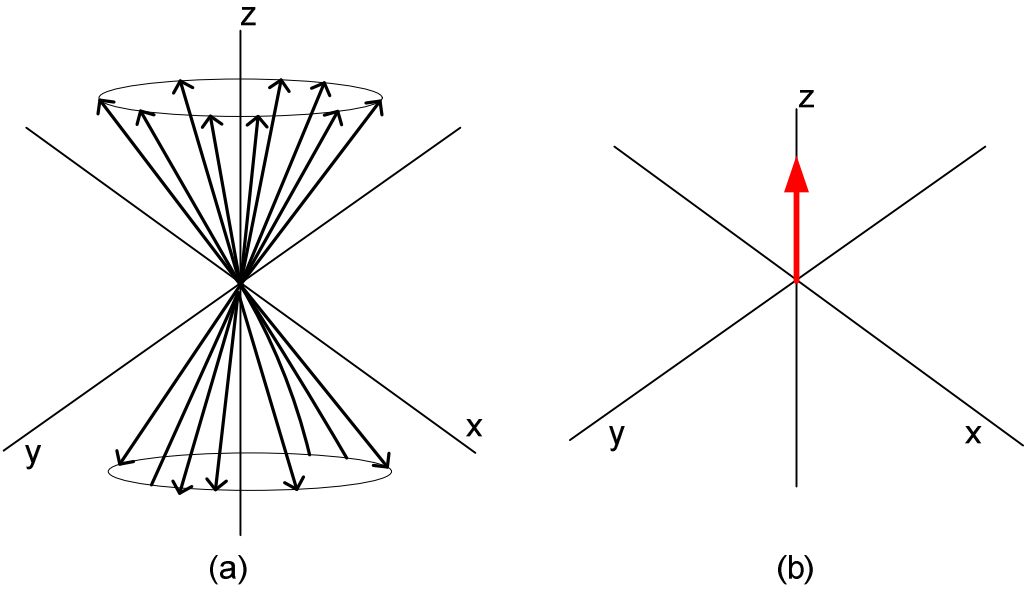

Figure 13: Equilibrium distribution of spins under an applied magnetic field, B_0. In the scheme, (a) denotes the individual spins and (b) is the net magnetization of the system.

Spins immersed in a magnetic field do not reveal much about the compound analyzed. Instead, we perturb the system and monitor its return back to equilibrium. This perturbation is accomplished by another magnetic field, most of the time with a 90^o angle. In the absence of the pulse, we observe a *free induction decay* (fid).

1.7.1 THE NMR SPECTROMETER

A modern NMR spectrometer is a complex body. Its main components are a superconducting magnet, an RF console, probes and a computer. Figure 14 shows the components of an NMR spectrometer.

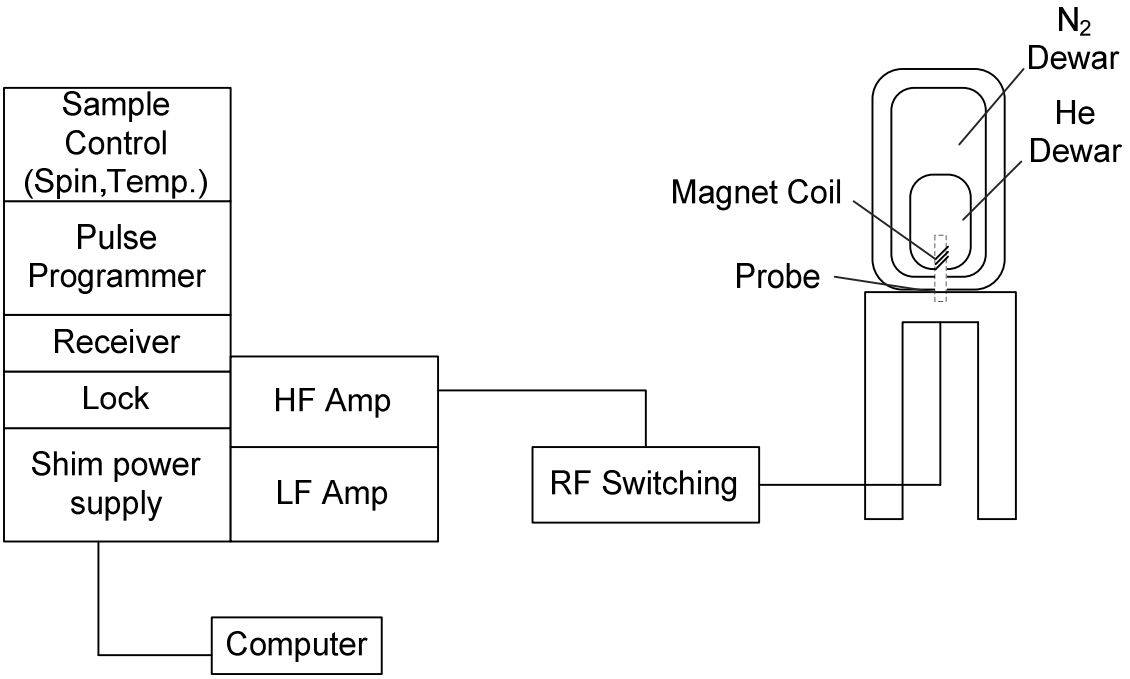

Figure 14: Represantation of NMR Spectrometer

1.7.1.1 The Magnet

A high-field superconducting magnet is an important component of this system. In order to make these superconducting magnets, superconducting metals are used.Since superconducting materials are able to conduct the electricity without producing any resistance, magnets made out of superconductors are able to provide high magnetic fields to the system.

1.7.1.2 Shim Coils

Having a good resolution in a NMR experiment is very crucial. The first thing that needs to be provided for a good resolution is a homogenous magnetic field. Shim coils are used for that purpose. Around 20 coils are added to the magnet. These coils have mostly different duties like spinning shims and non-spinning shims, but in modern spectrometers they are set up automatically.

1.7.1.3 RF Console

This part of the NMR spectrometer is the electronic part of the system. An RF console is working under a computer control and composed of amplifiers, pulse programmer, switches, gates and mixers. The way it works is as follows: Computer sends a signal and RF console gives a pulse by generating the proper frequency. It turns the RF transmitter on during the pulse length, amplifies the pulse and sends it to the probe. Receiver detects the signal and the computer stores it.

1.7.1.4 NMR Probe

NMR probes are devices that are inserted into magnet to keep the sample. They contain an RF coil. Pulses coming from the RF console are sent to the probe and the coil attached to it. Right after the pulses are transmitted, this same coil detects the free induction decay, fid. In most of the probes there are other electronic elements to detect the spinning rate and the temperature of the system. Probes also have heaters to warm the flowing air, nitrogen, to control the temperature of the sample.

Different probes are used for solid and solution samples. Probes for solution state NMR experiment fit into the bottom of the magnet by applying an air pressure. In order to provide spin homogeneity within the sample, another gas steam spins the sample at a frequency between 15-30 Hz. In solution state probes, there is another coil to tune the deuterium frequency. When a deuterated solvent is used during the signal acquisition, in order to provide the homogeneous field, the deuterium signal from the solvent is used as a field frequency lock.

NMR probes are designed to place a specific sample tube. In general, proton tubes are built to accept 5 mm NMR sample tubes.

1.7.1.5 Computer

Computers are the heart of the modern NMR spectrometers. Every component of the spectrometer is under the control of the computer. It is specialized to control high-speed functions. Basically it is responsible from application of RF pulses, control of the gates to send pulses to the probe, routing the NMR signals and collecting them back to computer for storage.

1.7.2 NMR Relaxation

Relaxation phenomena in NMR can be defined as the return of net magnetization back to equilibrium. Relaxation times are classified into two types: Spin-lattice relaxation (T_1), which is the precession of spins back to thermal equilibrium, and spin-spin relaxation (T_2), which describes the phase relation between interacting spins of solvent molecules [42].The relaxation times,T_1 and T_2, can be related to the molecular correlation times. In other words, the NMR relaxation of protons and their mobility are directly related, revealing information about the environment of protons.

1.7.2.1 Spin –Lattice (T_1) Relaxation

Spin-lattice or longitudinal relaxation can be described as the recovery towards the equilibrium state after some perturbation (i.e. RF pulse). If we assign the reference magnetization state as aligned along the *z*-axis, then we monitor the rate of return to alignment along the *z*-axis, and obtain the relaxation constant T_1. At equilibrium, the net magnetization vector (M_0) aligns with the applied magnetic field (B_0). In this configuration the *z* component of magnetization (M_z) is equal to (M_0). As there are nomagnetization contributions from the transverse *x*and *y*directions, M_x and $M_y$are both equal to 0 [43]. The equilibrium configuration is shown in Figure 15a. When it is polarized with a 90° pulse in the

x-direction, net magnetization starts to lose its intensity in the *z* direction and all of the spins orient in the the x-direction. By the time we stop sending 90° pulse it starts to decrease gradually in the x direction as shown in Figure 15b, 15c and 15d.T_1relaxation proceeds via molecular motion.

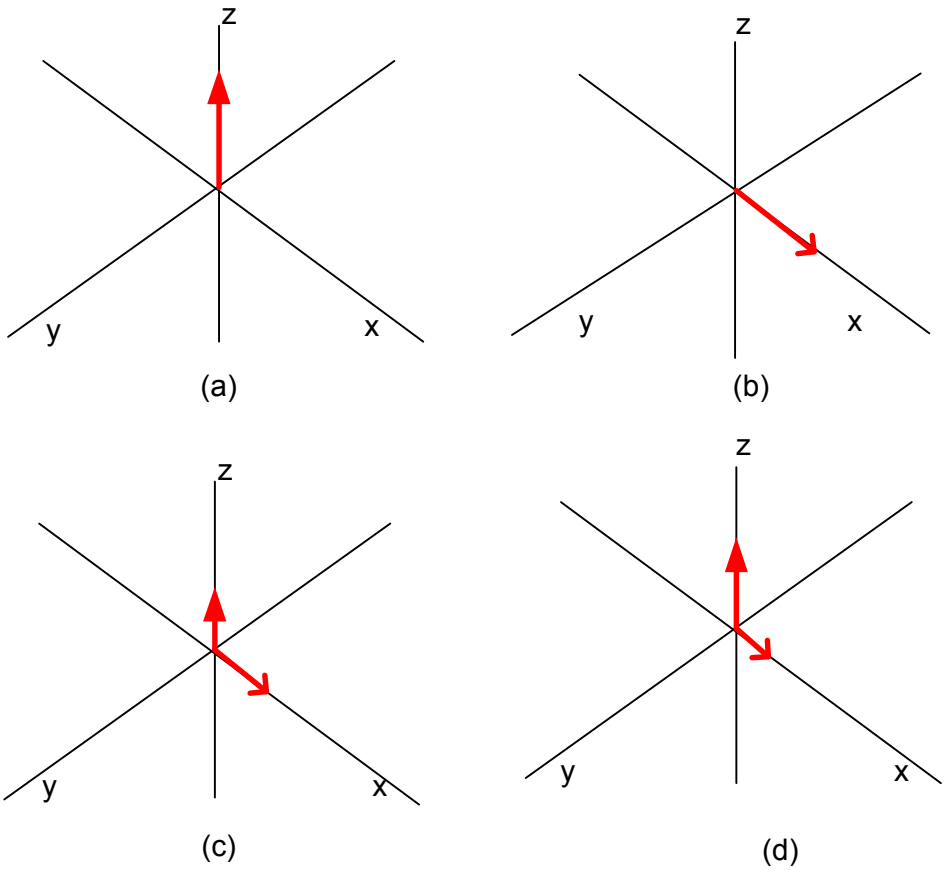

Figure 15: Representation of T_1 relaxation. The drawing shows (a) the net magnetization under an applied magnetic field, (b) as the 90^0 pulse is applied to the system in *x*-direction,(c) and (d) net magnetization gradually decays on*x* axis and grows onthe *z*-axis.

When this nucleus is polarized with a 90° RF pulse, it is possible to change the direction of the M_0 and make M_z= 0 if the system is provided enough energy (Figure 15 (b)). Once the 90° RF pulse is removed from the system, the spin system will recover toward equilibrium along

the *z* axis (Figure 15 (c)). Thus, the spin-lattice relaxation time is associated with how quickly M_z returns to its equilibrium value. Equation 12, gives the rate of relaxation.

$$M_z = M_0(1 - e^{-t/T_1}) \qquad \text{(Eqn.12)}$$

Inversion recovery is a common way to measure T_1 relaxation. Nuclei under an applied magnetic field are inverted 180° upon application of another magnetic field, which rotates the net magnetization to the *–z* axis. After a relaxation delay (before the system reaches equilibrium), the system is polarized by the application of an orthogonal pulse. At this step, the system rotates to the *xy*-plane. Once the net magnetization is in transverse plane, it rotates about the *z*axis by giving a *fid* signal.

1.7.2.2 Spin- Spin (T_2) Relaxation

Spin-spin or transverse relaxation time measures the loss of magnetization in the transverse or *xy*-plane. Each spin has a different magnetic environment (*i.e.* they feel different magnetic fields around them), so that they precess at different Larmor frequencies. In spin-spin relaxation, net magnetization decreases due to decoherence between neighboring spins precessing at different Larmor frequencies. This is most easily seen in projection onto the transverse plane.

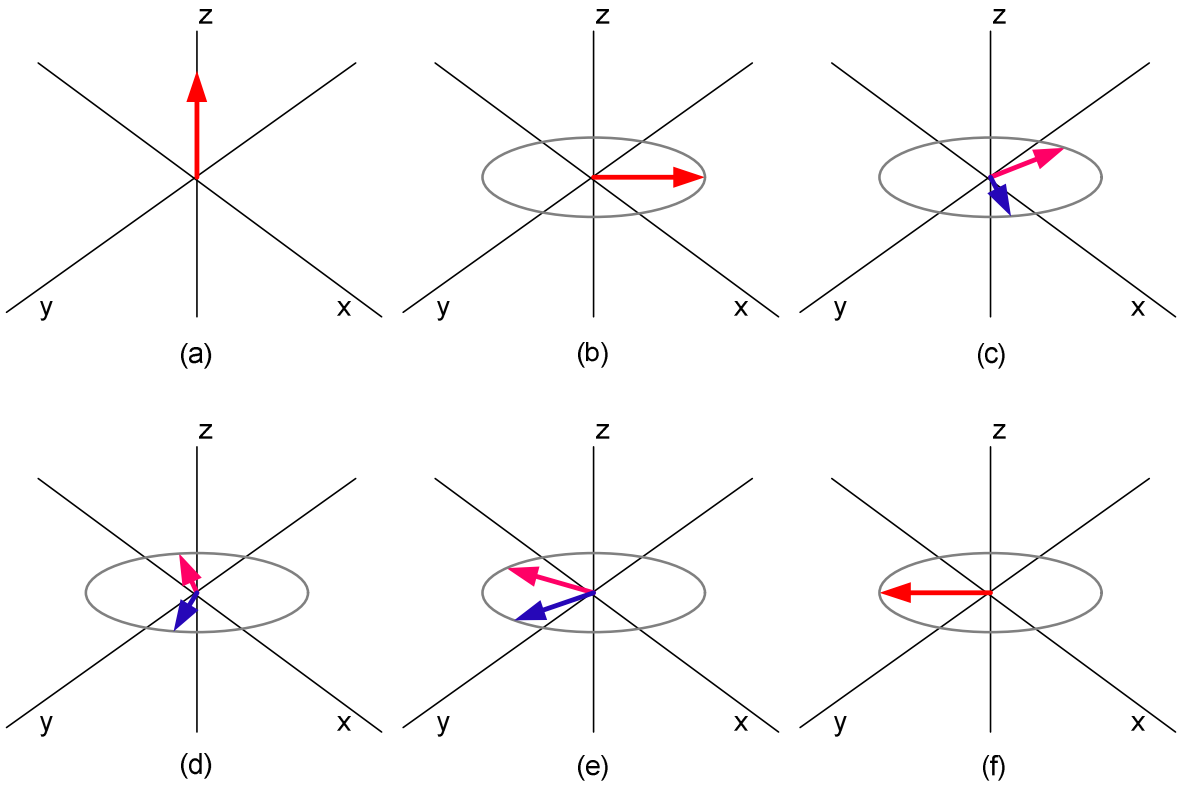

Figure 16: Schematics showingof T_2 relaxation and echo sequences. The drawing shows, (a) the net magnetization, (b) spin's reorientation after a 90° pulse is applied, (c),(d) and (e) how spins cannot keep up with each other and start to dephase on the transverse plane. (f) spins come in phase again after a 180° pulse is applied.

The basic pulse sequence to measure the T_2 relaxation rate is 90°-τ- 180°-τ. A 90° pulse rotates the magnetization to *xy*-plane. At this point the spin projection onto the transverse plane reveal decoherence [43]. When a 180° pulse is applied after some time, magnetization rotates by 180°, and this helps the system recover coherence to some extent and produces an echo. The aim of applying a 180° pulse is to make slower spins to come to the front (i.e. positions of individual spins will change), and this will facilitate the recovery of coherence.

As the local environment of a molecule determines the relaxation dynamics, the time-domain NMR response, *i.e.* the pre-Fourier transformed free induction decay, can be used to discriminate between highly mobile (*i.e.* liquid-like molecular bonding) and highly immobile (*i.e.* solid-like molecular bonding) protons [36].

In a solution of polymer-functionalized colloidal particles, the protons of the polymer are also interacting with those of the solvent, so the relaxation dynamics of the solvent molecules can also be probed, in addition to those of the macromolecule [37].When a solvent molecule is free, its relaxation is on the order of several seconds. However, if it is trapped within a polymeric environment, isotropic molecular motion would not be permitted, and the relaxation time will be much shorter. Thus, in analyzing the relaxation dynamics of solvent molecules, we can determine the relative mobility, which would indicate if the molecule is entrapped or free.

However, tracking only the solvent molecules is not sufficient, since the detected signal also contains responses from the protons of the polymer in the system. By designing a pulse sequence to suppress certain responses, the bound polymer fraction can be estimated [44]. Solid and liquid spin-echo experiments have been conducted to probe the polymer that is adsorbed onto the surface of nanoparticle, confirming that there is a distinct correlation time difference between fully bound polymers (*i.e.* via numerous segments in a "train"-like conformation) and the ones with a majority of segments well-solvated (*i.e.* "tail"-like) [45]. The ones that are lying on the particle surface have longer correlation times, whereas in the tail-like state, the correlation times are significantly reduced [44].

To detect the polymers adsorbed at the solid-liquid interface, solid and liquid echo experiments have been used. The adsorbed polymer exists in two different physical states with distinct correlation times. Train conformation, refers to the adsorption of a sequence of segments on the particle surface. In this physical state, the correlation time is longer. The

second physical state refers to parts of polymer chains that are solvated and have shorter correlation times.

To separate these two physical states from each other, two pulse sequences can beapplied:A conventional spin-echo sequence (90°_{x}-τ-180°_{y}) and a sold-echo sequence (90°_{x} -τ- 90°_{y}). And the intensity of these two echoes' heights were compared. The significance of these sequences is that, in solid-echo, both dipolar averaged and dipolar coupled populations are refocused, but in a spin echo experiment, only former spins are refocused. To explain this situation clearly, the effect of pulses of different lengths on dipolar Hamiltonian (H_{DD}) can be considered. In Equation 13, *i* and *j* are given as nuclear pairs,

$$H_{DD} = \frac{A}{r^3_{ij}}(1-3\cos^2\theta_{ij})(I_i * I_j - 3I_{iz}I_{jz}), \qquad \text{(Eqn.13)}$$

where A is a constant, r_{ij} is the internuclear separation, I is the spin vector and θ_{ij} is the angle between r_{ij} and the applied magnetic field. When the system is polarized with a 90^{o}, pulse all the spin states mixes (*i.e.* $I_x \rightarrow I_y$). A 90^{o}pulse can cause the spin terms to cancel each other under appropriate conditions. 180^{0} pulse inverts the spin vectors (*i.e.* $I_x \rightarrow I_{-x}$), and produces no net effect on the $H_{DD.}$ An appropriate combination of closely spaced pulses (90^{o}_{x} -τ- 90^{o}_{y}) completely refocuses the strongly dipolar coupled *fid*. To refocus, the weakly coupled *fid*s, a combination of $90^{o}$and 180^{o}pulses, can be used. The sequence proposed by Cosgrove is 90^{o}_{x} - τ- 90^{o}_{y} - 2τ -90^{o}_{y} - 2τ-180^{o}_{y} - 2τ-180^{o}_{y}. The two 90^{o}_{y} pulses acts as a compensated pair for liquid signals. The necessity for two 180^{o}_{y} signals is due to presence of solid signals in liquid echo [45].

1.8 Hypothesis for this work and Methodology

A model system for such a study is poly-vinylpyrrolidone (PVP)-functionalized ZnO colloidal nanoparticles dissolved in 1-propanol. The strong affinity of the pyrrolidone group of PVP for the Zn^{2+}cations is driven by electrostatic attraction, for which many segments of the same macromolecule may adsorb onto the colloid surface train-like, as opposed to adsorbing at only one end tail-like. Thus, we have applied dynamic NMR techniques to analyze solutions of PVP-functionalized ZnO colloidal nanoparticles in order to elucidate the adsorption of the PVP macromolecules.

2 Experimental

2.1 Materials

Poly-vinylpyrrolidone was purchased from International Speciality Products. The chemical structure of the polymer is given by Figure2. The average molecular weight for polymer is 40.000 g/mol, K-30. Zinc acetate dihydrate ("$ZnAc_2$", $Zn(CH_3COO)\cdot 2H_2O$) (>99%) sodium hydroxide (> 97%) were purchased from Merck. The synthesis solvent, 1- propanol (>99.5%) was also purchased from Merck.

2.2 PVP- Functionalized ZnO Synthesis

(PVP)-functionalized ZnO colloidal nanoparticles were synthesized by reacting 4.6mM $ZnAc_2$ solution in 1-propanol with 0.02 M sodium hydroxide in 1-propanol alcohol in the presence of PVP K-30 dissolved at 3 concentrations: 0.11 g/mL, 0.07 g/mL and 0.05 g/mL. $ZnAc_2$ was first dissolved completely in PVP-containing propanol solvent the under vigorous

stirring at 70°C. After the addition of the sodium hydroxide, the solution at 70°C was stirred for 4 minutes, and then quenched in an ice bath.

2.3 Post Processing After Synthesis

To eliminate the excess (*i.e.*, non-adsorbed) polymer in all of the systems, solutions were centrifuged at 125,216 × g (Beckman Coulter Opima Max TL) at 18°C for 1.5 hours with a fixed angled rotor (TLA-110).

2.4 Characterization

2.4.1 Fourier Transform Infrared Spectroscopy (FTIR)

In order to control if PVP is coordinated with the surface of ZnO nanoparticle, Fourier Transform Infrared Spectroscopy (FT-IR) measurements were made (Thermo Scientific, Nicolet IS 10). A sample with only PVP dissolved in propanol and another sample with 0.05 g/mL PVP-functionalized colloidal ZnO's FTIR spectra were compared. The resolution was reduced to 1 and sample collection amount was increased to 64 in order to be able to track smaller shifts in the FTIR spectra.

2.4.2 Photoluminescence Measurements (PL)

To elucidate the electronic structure of colloidal ZnO nanoparticles photoluminescence (PL) measurements were done. Disposable, polystyrene cuvvettes were used for measurements. The sample is illuminated using a HeCd laser (λ_{ex}= 325nm, KIMMON) and the detector is fluorescence specific spectrometer (Ocean Optics USB4000-FLG). We used a homebuilt system of our own for PL measurements.

2.4.3 UV-Visible Absorption Spectroscopy

The bandgap of the ZnO colloids was extrapolated from the absorption onset using UV-Visible (optical) absorption spectroscopy (Shimadzu, UV-3150, Kyoto, Japan). Quartz cuvettes were used in order to prohibit any possible absorption by cuvettes.

2.4.4 Dynamic Light Scattering

The hydrodynamic radius of the functionalized nanoparticles was determined by dynamic light scattering (ZetasizerNanoZS, Malvern Instruments, Malvern, UK). Standard disposable poly(styrene) cuvettes were used for measurements. The detector was fixed at the scattering angle of 173° (the Noninvasive Backscattered optical detection technology maximizes the sample volume analyzed, enabling study of a broader range of particle sizes and concentrations), and a HeNe laser was used as a light source with λ = 632 nm. Characterization was performed at 23 °C (room temperature) waiting for 2 minutes for temperature equilibration. For optical parameters, although covered with PVP, ZnO was taken as core of material. Since most of the polymer is eliminated with the centrifuge, the viscosity of the system is set to 1-propanol's viscosity.

2.4.5 Nuclear Magnetic Resonance

To determine the conformation of the polymer adsorbed on the nanoparticles, dynamic NMR methods were used. The functionalized nanoparticle samples (100 μL) were dissolved in 0.5 mL of deuterium oxide (D_2O, 99.9%). NMR spectra were collected using a Varian Unity Inova 500MHz spectrometer (Varian Unity Inova, Palo Alto, CA USA). The spectra were recorded at room temperature with a 500 MHz, 1H-19F (15N-31P), 5 mm PFG, Switchable Probe.

2.4.5.1 ^{1}H NMR

Proton NMR spectra were acquired using custom solid and spin-echo sequences (32k data points, acquisition time 1.892 s, 90° pulse of 13.2 μs width, 10 s repetition delay (τ), and integrated over 16 scans). The first pulse sequence used was $90°_x$–τ–$90°_y$–2τ, followed by another sequence $90°_y$ –2τ–$180°_y$– 2τ–$180°_y$–2τ.

Chemical shifts were referenced with respect to the resonance of water at 4.8 ppm. T_1 and T_2 characteristics were recorded.

2.4.5.2 ^{13}C NMR

The 1D carbon NMR spectra were acquired using S2PUL sequence with proton decoupling (spectral width 32 KHz, acquisition time 1.3 s, 90 degrees pulse width of 10 μs, pulse delay time 5s.

2.5 Nucleation of ZnO

Another set of experiment was designed in order to deduce the contribution of PVP into nucleation and growth of colloidal ZnO nanoparticles. This experiment was repeated for 2 different polymer concentrations: 0.11 g/mL and 0.05 g/mL. In the first group, only PVP in the given 2 concentrations was dissolved in the propanol solvent. In the second group, again the same amount of PVP is dissolved in 4.6mM zinc acetate in propanol solution. The change in the hydrodynamic radius with the addition of the cation into the system was tracked. Hydrodynamic radius was determined again with DLS.

2.6 Calculating the Surface Area of Particles

Using the nanoparticle radius extrapolated from absorption spectroscopy in the visible light spectrum (Table 3), the average surface area per particle was calculated. The number of particles that are formed for each concentration was estimated from the ratio of the total volume of ZnO to the volume of a single ZnO nanoparticle, assuming that all of the reactants have been consumed to form particles. After normalizing the intensity, the surface area can be calculated by assuming a Gaussian particle size distribution. The standard deaivation for absorption spectroscopy is estimated by correlating the standard deviation from hydrodynamic radius measurements. The total surface area of the particle population can then be obtained by multiplying the number of particles with the average surface area of a particle.

3 RESULTS

In order to estimate the particle size, we used two complementary techniques, UV-visible absorption spectroscopy and dynamic light scattering. From absorption spectra, the relative shift in band gap due to quantum confinement can be correlated to the particle radius, r. By extrapolating the linear part of the absorption onset to zero absorption [46], the band gap of the colloidal nanoparticles, E_g^*, was determined and compared to the band gap of bulk ZnO, E_g^{bulk}, for which we used a value of 3.2 eV was used [47]. The other material parameters—free electron mass, m_0, permittivity of vacuum,ε_0, Planck's constant, h, ($2\pi\hbar$), the effective mass of a conduction band electron (m_e^* = 0.26 for ZnO),[47] the effective mass of a valence band hole (m_h^* = 0.59 for ZnO),[47] and the DC dielectric response (ε_r = 8.5forZnO),[47]—can all be related through Equation 14:[46]

$$eE_g^* = eE_g^{bulk} + \frac{\hbar^2\pi^2}{2r^2}\left(\frac{1}{m_0 m_e^*} + \frac{1}{m_0 m_h^*}\right) - \frac{1.8e^2}{4\pi\varepsilon\varepsilon_0 r} - \frac{0.124e^4}{\hbar^2(4\pi\varepsilon_r\varepsilon_0)^2}\left(\frac{1}{m_0 m_e^*} + \frac{1}{m_0 m_h^*}\right)^{-1} \quad \text{(Eqn. 14)}$$

By analyzing the DLS of particle mobility in a suspension, we determined the average hydrodynamic radius of the nanoparticles. Table 3summarizes the average hydrodynamic radius of the particle population that had precipitated in the different polymer concentrations investigated. The size of the nanoparticles decreased during nucleation and growth in increasing polymeric concentration.

Table 3: Summary of particle size measurements by absorption spectroscopy and dynamic light scattering

Concentration [g/mL]	Absorption Onset (nm)	Calculated Diameter (nm)	Error Bars (UV-vis)	Hydrodynamic Diameter (nm)	Error Bars (DLS)
0	357.56	5.48	0.018	182	0.7
0.05	337.89	4.18	0.018	5.86	1.36
0.06	337.12	4.14	0.018	5.4	0.15
0.07	336.51	4.12	0.015	4.97	0.98
0.09	332.44	3.94	0.018	4.74	0.45
0.11	325.54	3.68	0.018	4.15	0.98

As shown in Fig. 17, the carbonyl bond of PVP (C=O) has a resonance at 1659 cm^{-1}, which was observed by FT-IR (Fig.17). When ZnO was synthesized in the presence of PVP, the resonance of the C=O in PVP shifted to 1665 cm^{-1}, indicating that PVP had coordinated with ZnO.

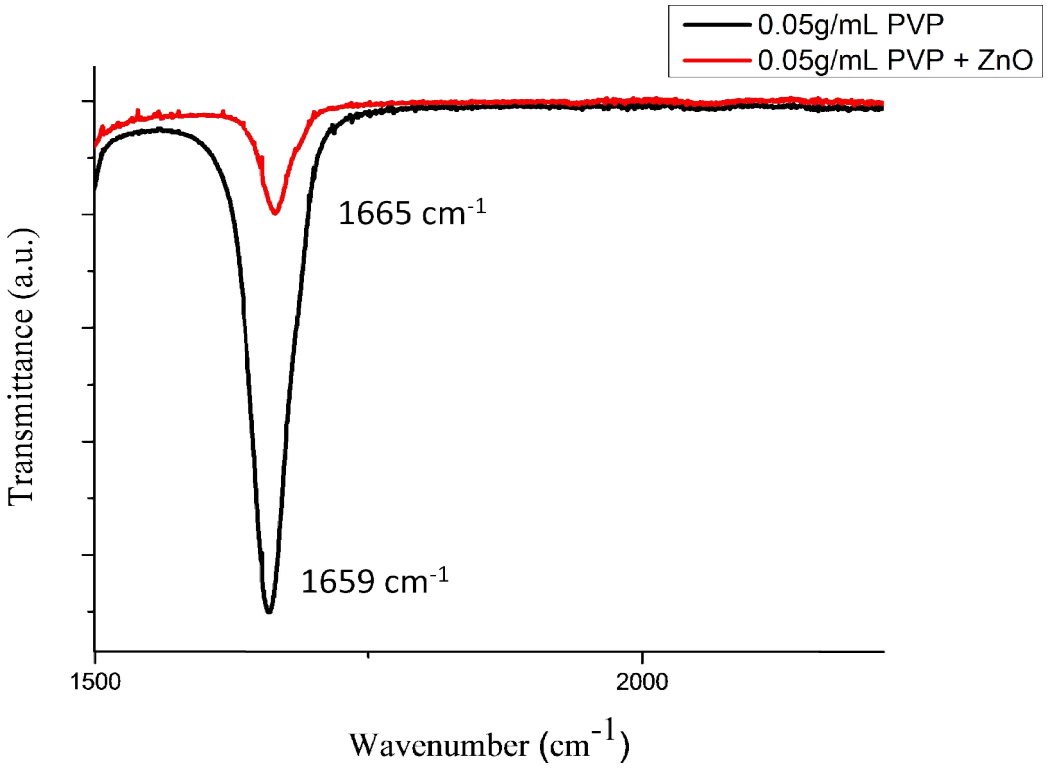

Figure 17:FTIR spectra of only PVP and 0.11 g/mL PVP functionalized ZnO nanoparticles

Photoluminesence (PL) measurements were done for threedifferent polymer concentrations. Two distinct peaks were observed for each concentration (Figure 18). The first peak is around 400 nm and the second peak is around 500 nm. As the concentration of the polymer is increased, we see a decrease in the intensity of the second peak.

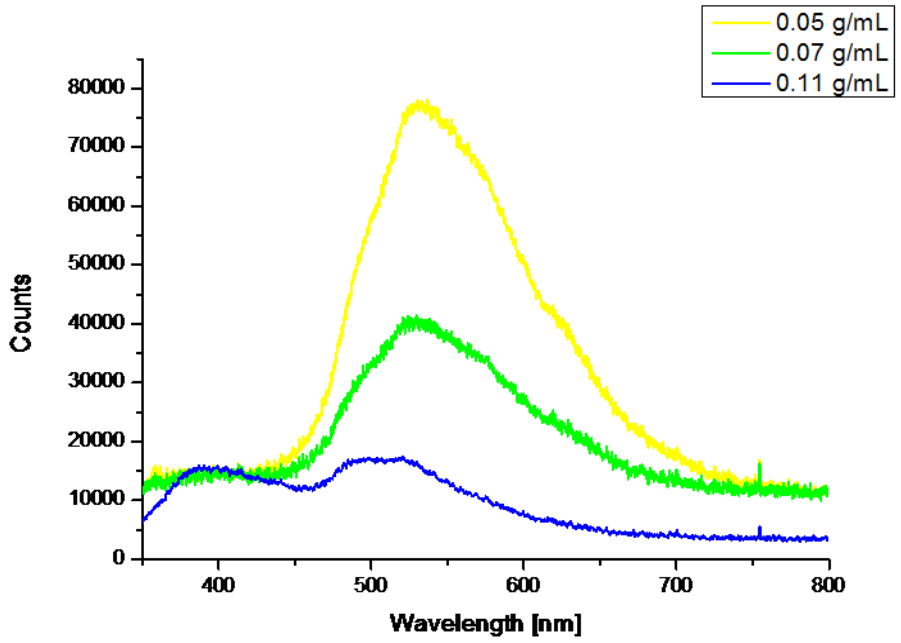

Figure 18: PL spectra of 0.05 g/mL, 0.07g/mLand 0.11g/mL PVP-functionalized ZnO nanoparticles

To characterize the chemistry of the polymeric colloid solution, proton (^{1}H) NMR analysis was performed. Figure 19 shows the ^{1}H-NMR spectra of the 0.11 g/mL PVP-functionalized ZnO nanoparticles dissolved in D_2O. Each carbon atom in the pyrrolidone ring is associated with a unique hydrogen atom, which is labeled according to their position in Fig. 20. As shown in Fig. 19, each pyrrolidone hydrogen nucleus reached resonance at chemical shifts consistent with the previous results of Sesta*et al.*[48]with the ^{1}H-NMR (PVP-functionalized ZnO nanoparticles in D_2O) peaks at δ_α= 3.64, δ_4 = 3.30, δ_2 = 2.31, δ_3 =2.01, δ_β = 1.73.

Figure 21 shows the full ^{1}H NMR spectrum of 0.11 g/mL PVP-functionalized ZnO nanoparticles dissolved in D_2O in order to have a clear view exactly which hydrogen nuclei are present in the system. To be precise, each hydrogen atom of the solvent propanol is labeled with a letter in Figure 22. The singlet peak at 4.8 ppm corresponded to the OH resonance of residual H_2O in D_2O, which was the solvent used for the NMR sample

preparation. The triplet at 3.58 ppm was associated with the CH_2 (labeled as A in figure 22) resonance, and the feature at 1.57 ppm was associated with the other the CH_2 (labeled as C in figure 22) of the propanol solvent (in which the colloidal particles were synthesized). Lastly, the other triplet at 0.88 ppm was associated with the $–CH_3$(labeled as D in figure 22) resonance of the propanol solvent. This peak normally appears around 0.96 ppm according to Spectral Database for Organic Compounds (SDBS) [49]. Although a chemical shift for the –OH resonance of propanol typically appears at 2.25 ppm, because the –OH of IPA can exchange with the D_2O, such a peak was not observed. Table 4 summarizes the identity and location of each resonance peak in the proton NMR spectrum.

(ppm)

Figure 19: Proton NMR spectra of the 0.11g/mL PVP-functionalized ZnO nanoparticles in D_2O. Peak labels correspond to the H associated with distinct locations in the vinylpyrrolidone mer.

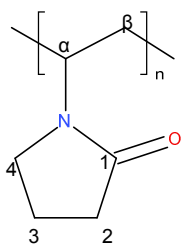

Figure 20: The structure of a vinylpyrrolidone mer

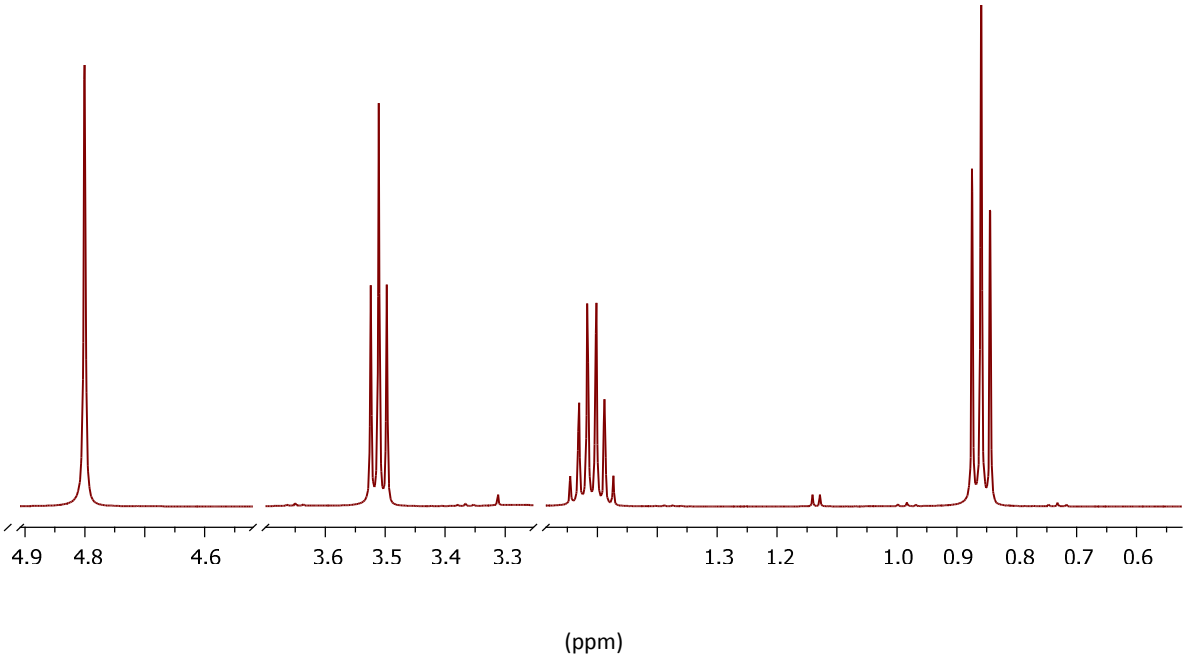

Figure 21: Full proton NMR spectra of the 0.11g/mL PVP-functionalized ZnO nanoparticles in D_2O.

Table 4: ^1H Chemical shifts of resonance peaks correlated to the solvent structure in 0.11 g/mL PVP-functionalized ZnO nanoparticles in H_2O

ResonancePeak	Chemical Shift ^1H (ppm)
-OH (water) $-CH_2$(A) $-CH_2$ (C)	4.8 3.582 1.57
$-CH_3$ (D)	0.88

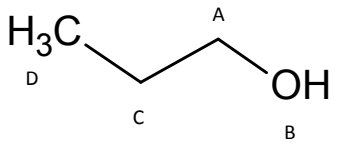

Figure 22: The structure of propanol molecule

To characterize the chemistry of the polymeric colloid solution, (^{13}C) NMR analysis was also performed. Figure 23shows the ^{13}C-NMR spectra of the 0.11 g/mL PVP-functionalized ZnO nanoparticles dissolved in D_2O. As shown in Fig. 23,each carbon of the pyrrolidone (Fig.20) reaches resonance at chemical shifts consistent with the previous results of Bergström, *et al*,[50]with the ^{13}C-NMR peaks at δ_1 =176.5, δ_α= 45, δ_4 = 43, δ_3 =18, δ_β = 35, δ_2 = 32.

Figure 24shows the full ^{13}C NMR spectrum of 0.11 g/mL PVP-functionalized ZnO nanoparticles dissolved in D_2O in order to monitor which carbons will respond to our dynamic NMR pulses. Three distinct singlets were observed in the spectra. The one at 9.98 ppm is associated with the $–CH_3$ resonance (labeled as D in Fig.22), 25.9 ppm peak is associated with the $–CH_2$resonance (labeled as C in Fig.22) and last one is at 64.25 ppm is associated with the other $–CH_2$resonance (labeled as C in Fig.22) of the propanol. Again in general, the peak at 9.98 ppm would appear at 10.28 ppm. Table 5 summarizes the identity and location of each resonance peak in the carbon NMR spectrum.

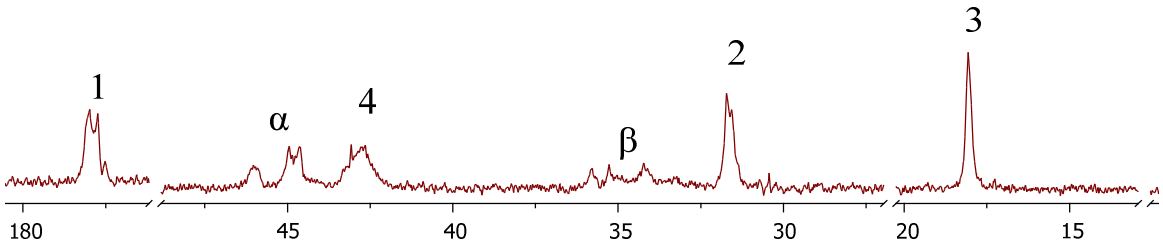

Figure 23: Carbon NMR spectra of the 0.11g/mL PVP-functionalized ZnO nanoparticles in D_2O. Peak labels correspond to the C associated with distinct locations in the vinylpyrrolidone mer.

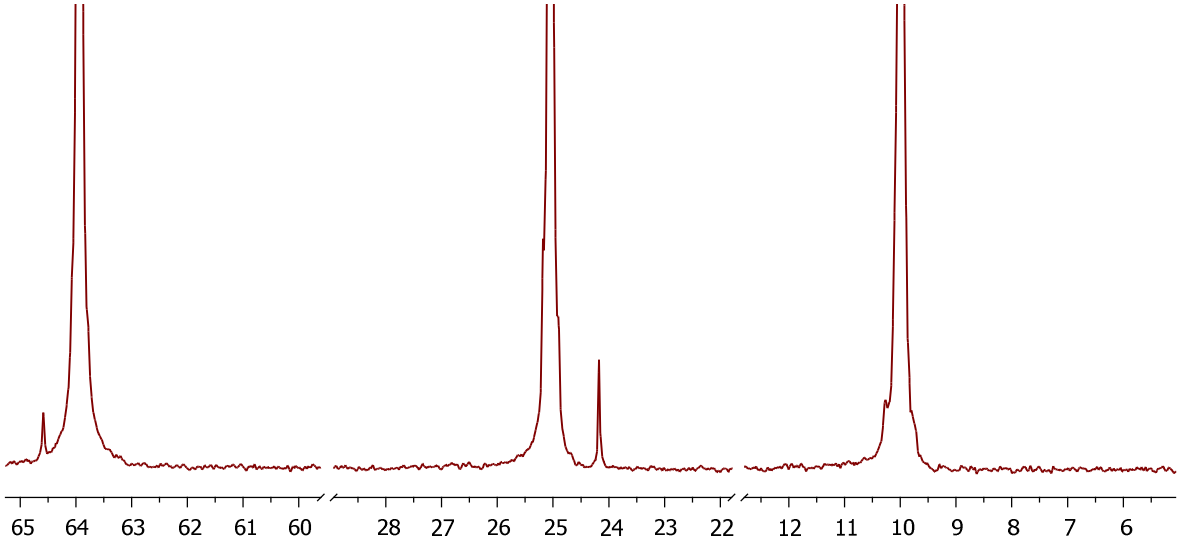

Figure 24: Full carbon NMR spectra of the 0.11g/mL PVP-functionalized ZnO nanoparticles in D_2O.

Table 5: ^{13}C NMR chemical shifts of resonance peaks correlated to the solvent structure in 0.11 g/mL PVP-functionalized ZnO nanoparticles in H_2O

ResonancePeak	Chemical Shift ^{13}C (ppm)
$-CH_2$ (A)	64.25
$-CH_2$ (C)	25.89
$-CH_3$ (D)	9.98

Both the spin-lattice interaction dynamics (represented by theT_1 value) and the spin-spin interaction dynamics (represented by T_2) of the solvent were also monitored for the PVP-functionalized nanoparticles that had precipitated in each different polymer concentration. For each of the ^1H resonance shifts of solvent molecules identified above (Fig.21 and Table 4), a decreasing trend for T_1 relaxation response to the pulsed NMR field correlating with polymer concentration, as summarized in Table 6 is observed with the increasing polymer concentration. In the case of the T_2 response, only the $–CH_2$and $–CH_3$ showed a discernible increasing trend with varying functionalizing polymer concentration (Table 7).

Table 6: ^1H NMR T_1 relaxation of the propanol and water molecules in units of seconds

Concentration [g/mL]	4.8 ppm	3.5 ppm			1.5 ppm		0.86 ppm		
		a	b	c	a	b	a	b	c
0.05	8.54	4.379	3.825	3.363	4.128	4.256	3.971	3.474	3.113
0.07	8.016	3.903	3.704	3.706	3.989	3.954	3.469	3.452	3.139
0.09	7.437	3.067	2.023	2.31	2.621	2.961	1.775	2.779	2.155

0.11	7.282	3.099	3.926	3.349	3.61	3.736	3.17	3.42	2.562

Table 7: ^{1}H NMR T_2 relaxation of the propanol and water molecules in units of seconds

Concentration [g/mL]	4.8 ppm	3.5 ppm			1.5 ppm		0.86 ppm		
		a	b	c	a	b	a	b	c
0.05	0.3899	2.607	2.756	2.919	3.283	3.251	2.874	3.638	2.817
0.07	0.6015	3.163	3.315	3.06	3.328	3.393	3.071	3.401	3.468
0.09	0.487	3.412	3.454	3.144	3.442	3.598	3.046	3.404	2.885
0.11	0.4597	3.471	3.676	3.11	3.589	3.721	3.13	3.728	3.2

The ^{13}C resonance shifts were identified for each C in the propanol molecule in Fig.24and Table 5, in addition to both spin-lattice and spin-spin relaxation characteristics. For both $T_1$and T_2 relaxation times, we observed an increasing trend with increasing polymer concentration (Tables9).

Table 8: ^{13}C NMR T_1 relaxation of the propanol moleculein units of seconds

Concentration [g/mL]	63.95ppm	25.02ppm	9.98ppm
0.05	5.31	5.599	6.428

0.07	5.453	5.523	6.596
0.11	5.502	5.602	6.707

Table 9: ^{13}C NMR T_2 relaxation of the propanol moleculein units of seconds

Concentration [g/mL]	63.95ppm	25.02ppm	9.98ppm
0.05	1.574	1.64	2.419
0.07	2.641	2.478	3.683
0.11	3.226	3.605	3.839

To understand the role of the macromolecule in the nucleation of colloidal ZnO nanoparticles, twocomparable hydrodynamic radius measurements were done for two distinct PVP concentrations 0.05 g/mL and 0.11 g/mL. In the first set, hydrodynamic radius of 0.11g/mL PVP dissolved in propanol and 0.11 g/mL PVP dissolved in 4.6mM $ZnAc_2$ in propanol was compared. In the presence of dissolved zinc cations (Fig.26), size distribution of polymer became narrower and the size of the polymer decreased.

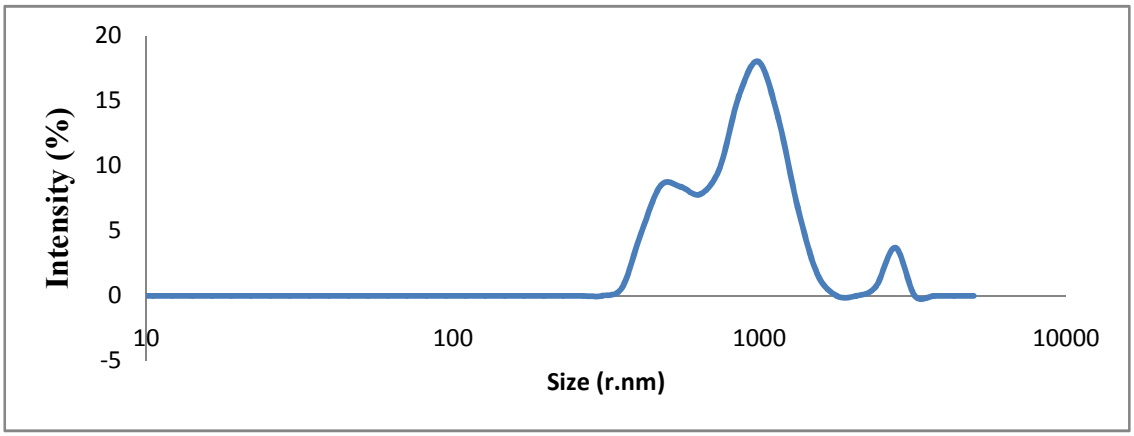

Figure 25: Hydrodynamic radius of 0.11 g/mL PVP dissolved in propanol

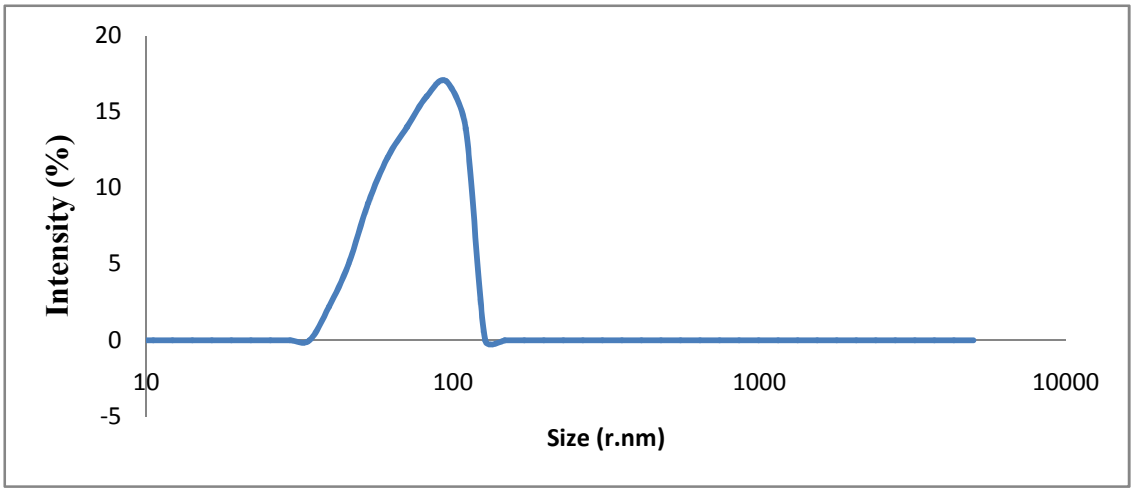

Figure 26: Hydrodynamic radius of 0.11 g/mL of PVP dissolved in 4.6 mM $ZnAc_2$ in propanol solution.

The same experiment was repeated for a 0.05 g/mL PVP concentration. The average hydrodynamic radius of the 0.05 g/mL PVP dissolved in propanol was measured as a uniform distribution below 10 nm (Fig.27). When 0.05 g/mL PVP was dissolved in 4.6mM of $ZnAc_2$ in propanol solution, again a uniform size distribution of hydrodynamic radius of PVP was observed, but this time the average hydrodynamic radius had become around 100 nm (Fig.28).

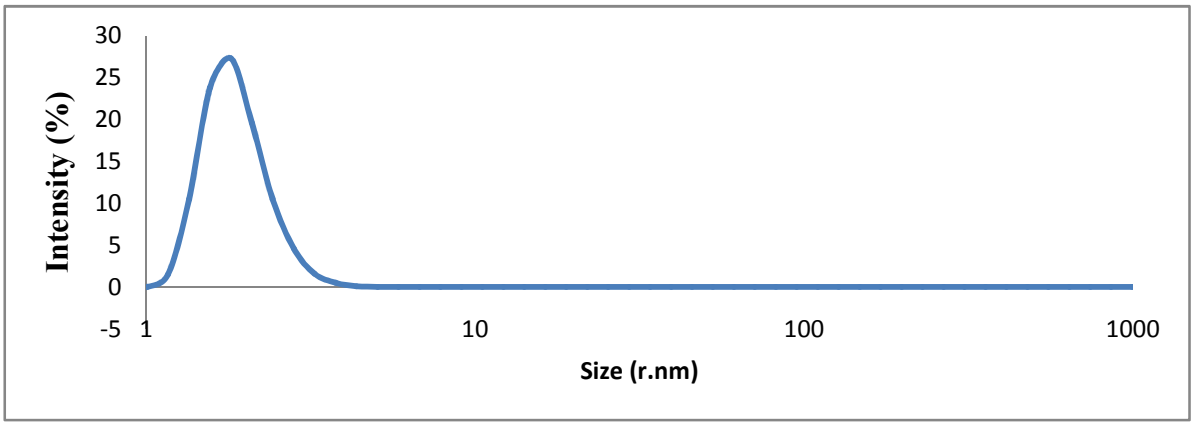

Figure 27: Hydrodynamic radius of 0.05 g/mL PVP dissolved in propanol

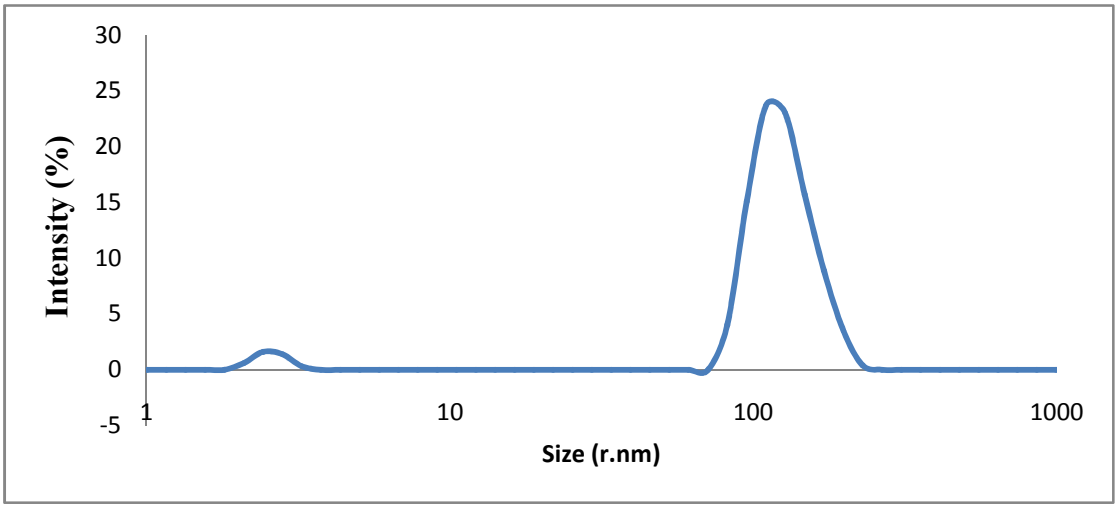

Figure 28: Hydrodynamic radius of 0.05 g/mL of PVP dissolved in 4.6 mM $ZnAc_2$ in propanol solution.

4 Discussion

PVP-functionalized ZnO nanoparticles remained more stable in solution (for longer than a month) than the non-functionalized particles. In contrast, non-functionalized ZnO particles had a strong tendency to agglomerate, as evidenced by the hydrodynamic radius of 91nm (Table 3), which was measured immediately following synthesis. In fact, the difference between the hydrodynamic radius and the particle radius extrapolated from absorption spectra (2.75 ± 0.03nm) was very large.

In addition to stabilizing the colloidal nanoparticles, the polymer macromolecules also appeared to define the colloidal nanoparticle size via their concentration. As shown in Fig. 29 and Table 3, the hydrodynamic radius increased with increasing polymer concentration at a faster rate than the particle radius extrapolated from absorption spectroscopy. This comparison suggests that the manner in which a polymer molecule adsorbs onto the surface of the ZnO may be changing with the growth environment as defined by the solution concentration.

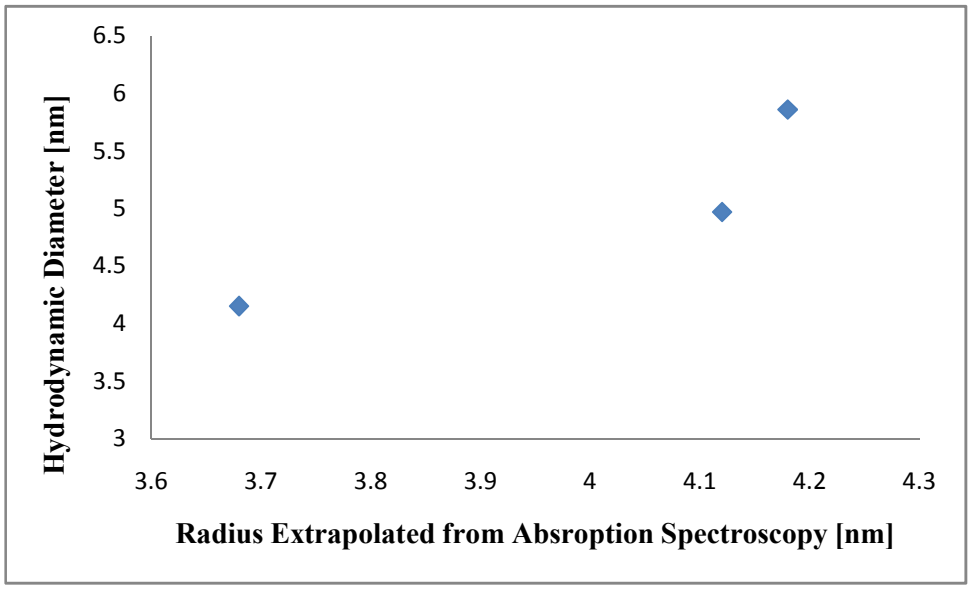

Figure 29: Hydrodynamic radius vs. particle radius extrapolated by absorption spectroscopy

We observed two distinct emission peaks for each concentration in the PL spectra (Fig.18). The first one was around 400 nm, close to the relaxation translation from conduction to valence band. The higher wavelength luminescence peak around 500 nm was consistent with de-excitation from surface trap states inside the band gap of ZnO [51,52]. Moreover, increasing the PVP concentration enhanced the interband emission but hindered emission from traps, suggesting that there were fewer available surface trap states on ZnO colloids synthesized in higher polymer concentration solutions.

Time domain NMR spectroscopy enabled us to elucidate the influence of polymer concentration on particle growth, by distinguishing the responses of individual ^{1}H nuclei to an applied magnetic field. As sample preparation for probing the NMR response necessitated combining the propanol solution of PVP-functionalized ZnO nanoparticles with deuterium oxide, the actual NMR sample consisted of PVP adsorbed onto ZnO nanoparticles, with the PVP molecules (and the exposed ZnO surface) well-solvated by propanol and some residual H_2O in the 99.9% pure deuterium oxide.

Both the ^{1}H and ^{13}C NMR results showed that CH_3 resonance of propanol (which is labeled as D in Fig. 22) appearedat lower ppm values than the expected range of pure propanol—normally the CH_3 resonance occurs at 0.96 ppm for^{1}H-NMR and 10.28 ppm for^{13}C-NMR [49]. Whereas in the case of the polymer-functionalized colloids,the CH_3 resonance appearedat 0.88 and 9.98 ppm, respectively,indicating shielding of thenuclei of CH_3 (*i.e.*, exposed to less magnetic field).

The ^{1}H-NMR response thus comes from the hydrogen nuclei of PVP, of propanol, and of H_2O. As the ^{1}H nuclear spin relaxation time of the $–CH_2$ for both A- and C-positioned hydrogen (see Fig.22), $–CH_3$ of propanol and –OH of water all decreased with increasing polymer concentrations, the loss of mobility in higher polymer concentration suggests that propanol and water molecules become less trapped (i.e. more mobile) in a denser polymer network.

Further insight into the system dynamics can be gleaned from the fact that the T_2-relaxation of propanol increased with increasing polymer concentration. Unlike T_1, which represents the spin-lattice interaction, T_2 represents the strength of coupling between nuclear spins in spin-spin interaction. Such an increase in T_2 is consistent with the motion of propanol molecules becoming less restricted in higher polymer concentration, whereas at lower concentrations, their motion was much more restricted. In contrast, the T_2-relaxation data of the H_2O molecules did not reveal a trend.

For particles in a PVP concentration of 0.07 g/mL, the T_2 value wasthe highest, indicating that water molecules were much more mobile within the system compared to denser environments—the residual H_2O molecules werenot able to access the particle surface due to exclusion by an adsorbed polymer layer, an effect that scaledwith polymer concentration. Denser polymeradsorption onto ZnO particlesentailedmore limitedaccess for water molecules to the particle surface.

From the perspective of the ^{13}C nuclei, the C of propanol displayed the strongest detectable response, as summarized in Fig. 30*a* and *b*. Although the spin-lattice (T_1) relaxation time increased with polymer concentration, the magnitude of change was very low, and possibly within the error bars. This indicates that at low polymer concentrations, propanol molecule has preferredorientationfor approaching to the surface of particles;however, as the polymer concentration increased, the variation became so small that we did not observe any directionality on propanol interaction with ZnO surface.On the other hand, the spin-spin (T_2) characteristics showed a clear trend of increasing time with increasing concentration, consistent with the proton NMR data, and confirming the reduced mobility of propanol with polymer concentration.

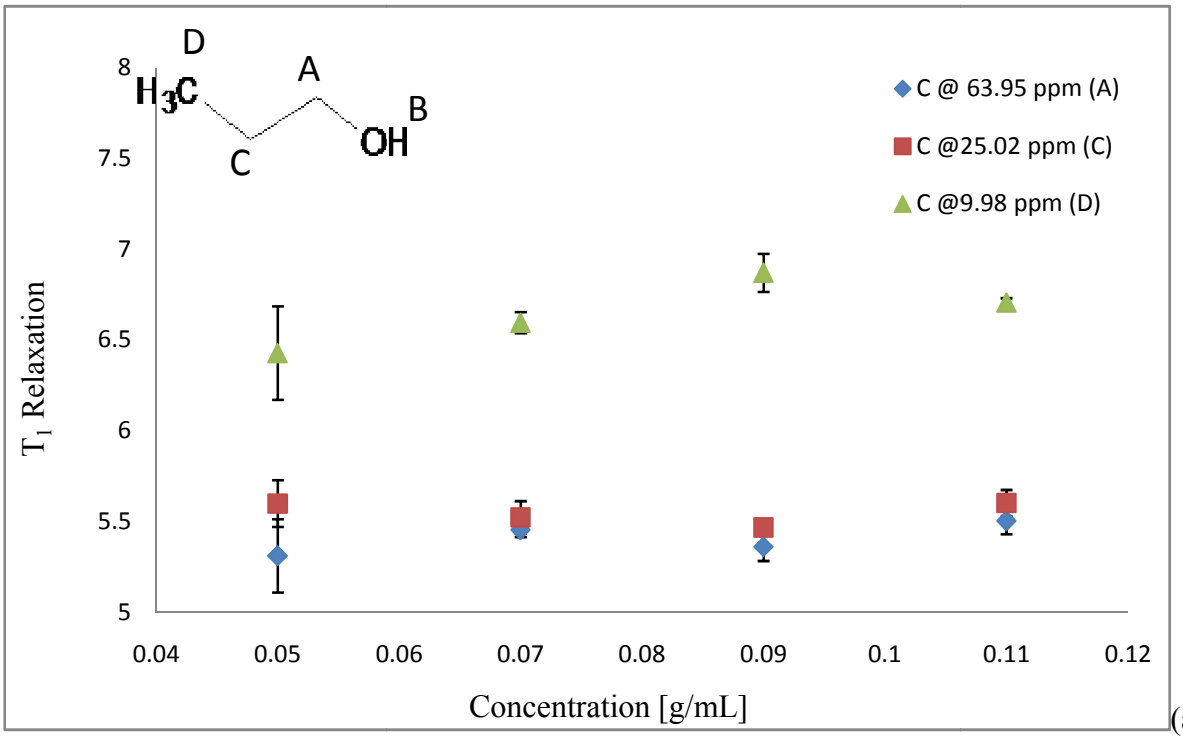

(a)

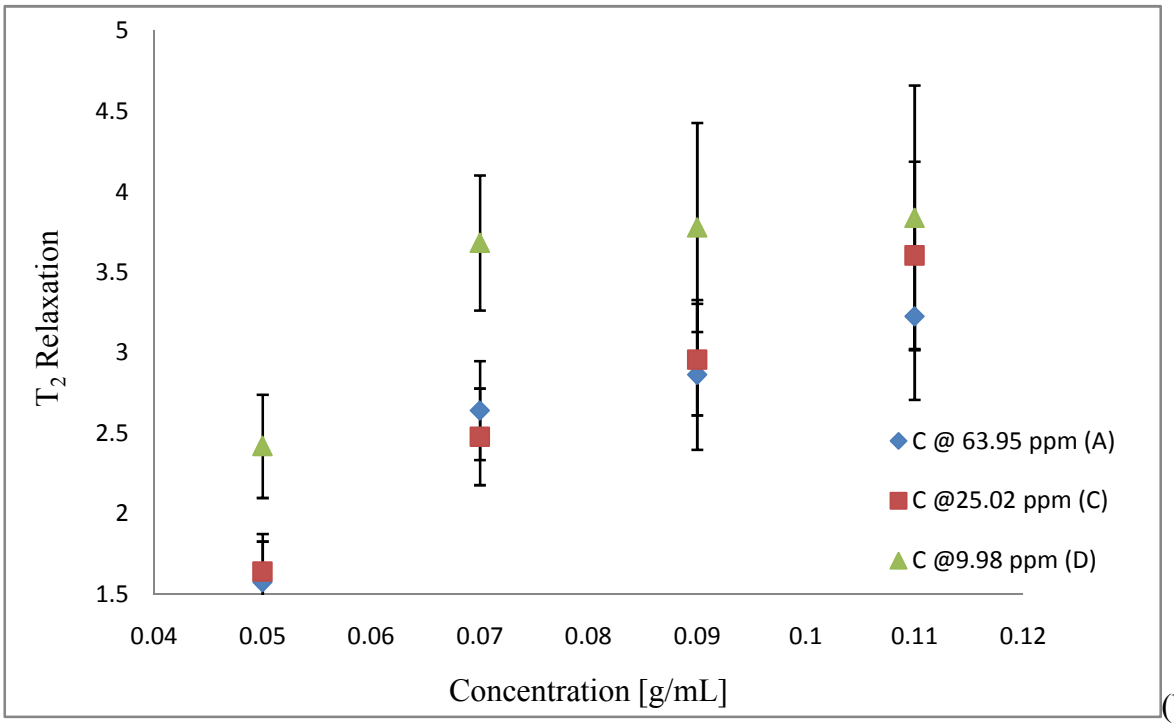

(b)

Figure 30: (*a*) T_1-relaxation characteristics for the PVP-functionalized ZnO, propanol, and deuterium oxide solution. The strongest detectable response came from the carbons of propanol, which are labeled in the inset figure; (*b*) T_2-relaxation characteristics for the PVP-functionalized ZnO, propanol, and deuterium oxide solution. The strongest detectable response came from the carbons of propanol, which are labeled in the inset figure.

Following the NMR-pulse sequence reported by Cosgrove, *et al*., we estimated the polymer bound fraction, $\langle p \rangle$, from the maximum of first echo, A, and the maximum of the last echo, B, using Equation 10.[45,53]

$$\langle p \rangle = 1 - B/A, \qquad \text{(Eqn. 10)}$$

The first pulse sequence, 90°_{x}– τ - 90°_{y} –2τ, where τ equals 10 microseconds, induced a response from protons throughout the entire system, *i.e.*, of both bound and non-bound polymers. This echo was followed by applying a second pulse sequence, 90°_{y} –2τ- 180°_{y}- 2τ- 180°_{y}- 2τ, to which only the protons of non-bound (*i.e.*, mobile) polymers respond. Polymer segments that were in close proximity to the surface of the nanoparticle were assumed to be bound polymers (*i.e.*, a partial bond between ZnO and pyrrolidone had formed). These segments exhibited the relatively low mobility of that in a solid, in contrast to freely solvated polymer chains.

The extracted <*p*> revealed that only the 5% of the polymer was adsorbed onto the surface of the ZnO nanoparticles, when synthesized in a PVP concentration of 0.05 g/mL. In a PVP concentration of 0.11 g/mL, 40% of the polymer had adsorbed onto the ZnO surface. However, when the ZnO particles were synthesized in a 0.07 g/mL PVP concentration, 80% of the PVP had adsorbed onto the ZnO surface. From the bound fraction experiment, we can conclude that PVP adsorbs with different conformation on the surface of nanoparticles, when solution polymer concentration is varied. Moreover, polymers at different concentrations contribute differently to nucleation of nanoparticles.

Table 10: Polymer bound fraction of 0.05 g/mL, 0.06 g/mL, 0.07 g/mL, 0.09 g/mL and 0.11 g/mL PVP-functionalized ZnO nanoparticles.

Polymer Concentration [g/mL]	<p>
0.05	0.05
0.06	0.03
0.07	0.81

0.09	0.12
0.11	0.42

Different sizes of particles offered different amounts of available surface area in the system. So, the bound fraction itself may not be so informative, if it is not normalized to the available surface area in the system. Figure 31shows the bound fractions per surface area. Again we observed that at 0.07 g/mL polymer concentration, more polymer had still adsorbed onto the unit surface area. At 0.05 g/mL polymer concentration, the lowest amount of adsorption had occurred at the unit surface.

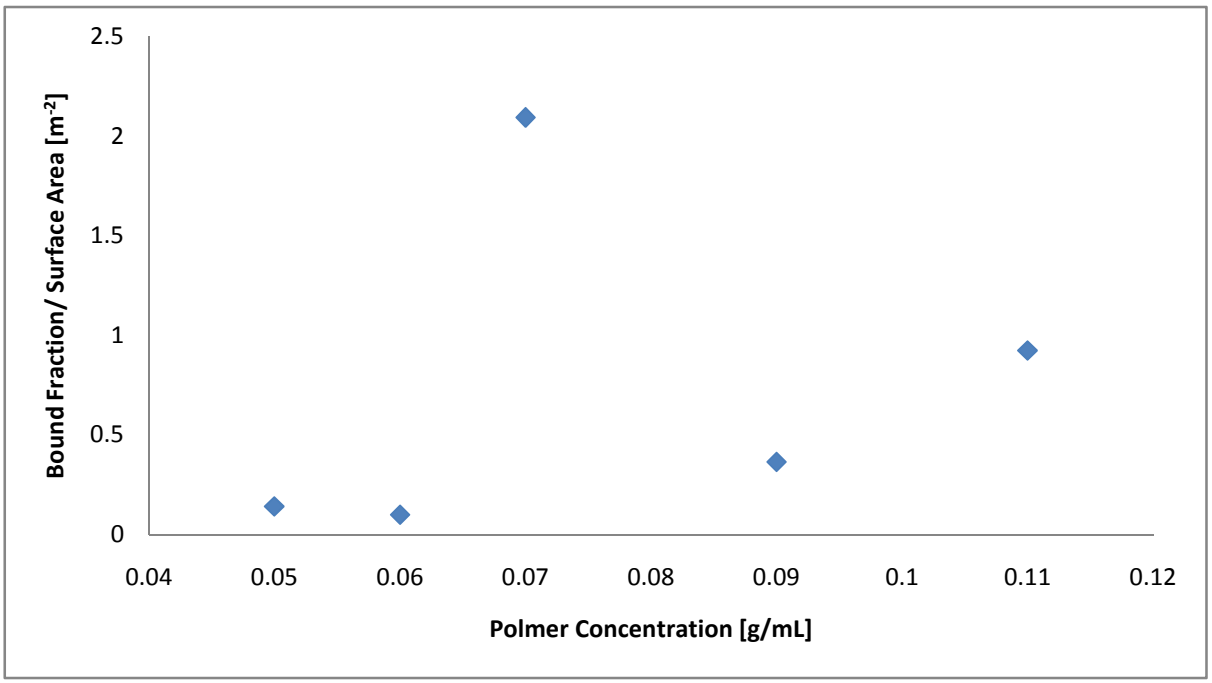

Figure 31: Bound fraction of functionalizing PVP per unit area

Time-domain NMR revealed that PVP was well-solvated by propanol at low PVP concentration, which is consistent with PVP adsorbing onto the ZnO surface in a tail-like conformation. In contrast, the poorer solvation by propanol at higher PVP concentrations correlatedwith more of the polymer adsorbing onto ZnO, indicating that the polymer conformation was more loop- or train-like.

4.1 Nucleation of ZnO nanoparticles in the presence of PVP

To elucidate how macromolecules contribute to nucleation of nanoparticles, the hydrodynamic radius of PVP in a propanol solution was measured and compared with the hydrodynamic radius of PVP in the presence of our precursor $ZnAc_2$molecules for two different polymer concentrations: 0.11 g/mL and 0.05 g/mL. At 0.11 g/mL polymeric concentration, a non-uniform distribution of PVP chains around 1000 nm in propanol solution was measured, suggesting that PVP macromolecules were forming large globules of interpenetratingchains (Fig.20). However, in the presence of $ZnAc_2$, the size distribution of the globules became more uniformly distributed around 100 nm (Fig.21), indicating that after coordinating with the C=O of PVP, the Zn^{+2}cations pulled these chains closer together. We observed a significant change in the R_g, consistent with Zn inducing densification of the PVP globules. In the first system, the highly concentrated polymer network formed globules with an R_g ~770 nm (Figure 27). However, in the presence of $ZnAc_2$, those polymer globules had densified to having an R_g around 77 nm (Figure 28). Also the coordination of Zn^{+2} and C=O of PVP createda partially positive charge on N atom. When NaOH was introduced to the system, this partial positive charge around N atoms attracted the OH^- anion with the electrostatic interaction and catalyzedthe nucleation of ZnO nanoparticles (Fig.32).

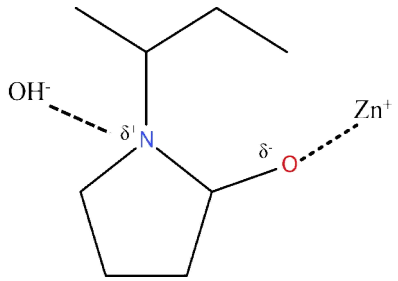

Figure 32: Electrostatic interaction of PVP with the addition of Zn^{+2} and OH^- sources.

At low polymer concentrations, PVP chains were well solvated and distributed in the propanol solution. Rather than forming large globules, they remained as distinct individual chains. Since they were not forming globules, a radius of interpenetrating globules could not be determined. The conformation of the PVP chains at low polymeric concentration depens on their lowest Gibbs free energy state. One possible conformation for PVP chains at low polymer concentraions is shown in Figure 35, where the blue dots present the solvent molecules around the polymer chain. Although propanol is a good solvent to dissolve PVP, a fully streched out conformation for PVP is not favorable due to entropic restrictions. When freely rotating chain model is applied to this system (Eqn. 2), with a C-C single bond length of 1.54 A^o and approximately 350 repeating units, the end-to-end distance of a single chain is calculated around 6 nm, which is also consistent with our experimental data (Fig. 27). When $ZnAc_2$ was introduced to the system, Zn^{+2} again coordinated with the C=O of PVP, and the PVP network began to densify, due to the electrostatics in the system.

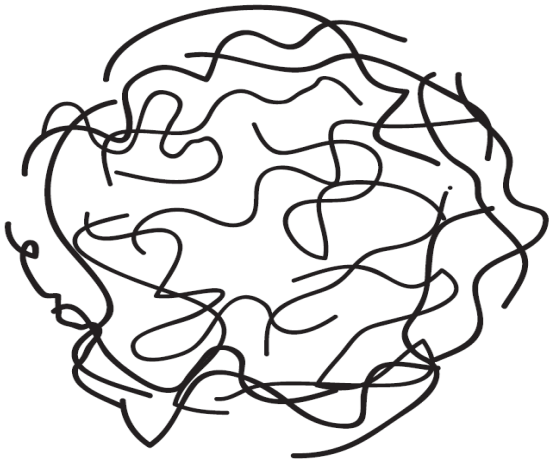

Figure 33: Schematic of an interpenetrating network of polymer chains at high polymer concentrations

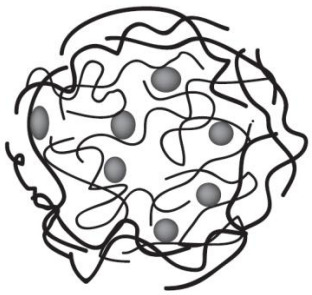

Figure 34: Schematic of an interpenetrating network of polymer chains in the presence of precursor at high polymer concentrations

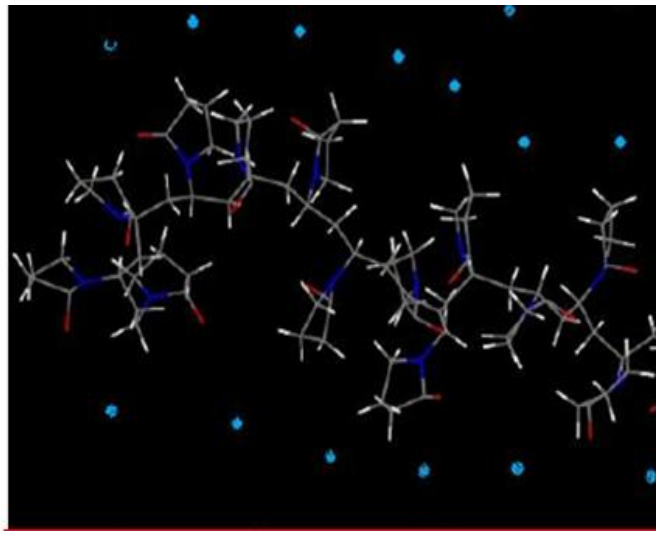

Figure 35: One possible conformation for single PVP chain at low polymer concentrations.

These results validate a model of highly dense polymer globules serving as reactors for ZnO nanoparticle precipitation, in which the high density of pyrrolidone rings in the globule hinders the diffusion of Zn^{+2} by electrostatic interaction. At high concentrations, large PVP globules appear to trap the reactant species and adsorb in a train conformation on the surface of precipitating ZnO nanoparticles. At low concentrations, the sizes of PVP globules are comparable to that of the evolving ZnO nanoparticles, and PVP adsorbs in looped and tail-

only conformation. Due to the relatively low interpenetrationof the macromolecule network, the polymer globules are largely extended and interact with the ZnO surface significantly less.

5 Conclusion

Dynamic (time domain) NMR techniques were used to determine how PVP adsorbs onto the surface of ZnO nanoparticles, via investigating the relaxation dynamics of the functionalizing macromolecules and the solvent molecules. The relative bound fraction, combined with particle size measurements and PL measurements indicated that the polymer concentration determinedthe conformation of the adsorbed macromolecule. Three different polymeric concentrations were chosenfor controlling the synthesis of ZnO nanoparticles. At a low polymer concentration of 0.05 g/mL, only 0.05% of PVP was adsorbed onto the surface of ZnO, whereas at a 0.07 g/mL PVP concentration, 80% of the PVP was adsorbed. Such a high bound fraction value implies that PVP may have adsorbed predominantly in a tail-like or loop-like conformation.Additionally, macromolecules participated in the nucleation of nanoparticles, when particles were synthesized in polymeric solutions. At high polymer 0.11 g/mL concentrations, the change in the radius of gyration of the interpenetrating polymer chains indicatedthat PVP exerteda templating role in nucleation of ZnO nanoparticles.

REFERENCES

[1] Julia H. Ding and Douglas L. Gin. Catalytic Pd nanoparticles synthesized using a lyotropic liquid crystal polymer template. *Chemistry of Materials*, 12(1):22–24, 2000.

[2] Ajay Kumar Gupta and Mona Gupta.Synthesis and surface engineering of iron oxide nanoparticles for biomedical applications.*Biomaterials*, 26(18):3995 – 4021, 2005.

[3] Lin Guo, Shihe Yang, Chunlei Yang, Ping Yu, Jiannong Wang, WeikunGe, and George K L Wong. Highly monodisperse polymer-capped zno nanoparticles: Preparation and optical properties. *Applied Physics Letters*, 76(20):2901–2903, 2000.

[4] Hussain, F., Hojjati, M., Okamoto, M., Gorya, R.E., Review article: Polymer-matrix

Nanocomposites, Processing,Manufacturing, and Application: AnOverview. *J. Compos. Mater,* 40 (17):1511-1559, 2006.

[5] Gonsalves, K. E., Chen, X., and Baraton, M-I., ìMechanisticinvestigation of the preparation of polymer/ceramic nanocompositesî, Nanostructured Materials, 9, pp. 181-184, 1997.

[6] Rong, M. Z., Zhang, M. Q., Zheng, Y. X., Zeng, H. M.,Walter, R., and Friedrich, K., ìStructure-property relationships of irradiation grafted nano-inorganicparticle filled polypropylene compositesî, Polymer, 42, pp. 167-183, 2001.

[7] Becker, C., Mueller, P., and Schmidt, H., Optical and thermomechanical investigations on thermoplastic nanocomposites with surface modified silica nanoparticles, Proc. of SPIE Conference on OrganicInorganic Hybrid Materials for Photonics, San Diego, 1998.

[8] T. Ramanathan, S. Stankovich, D. A. Dikin, H. Liu, H. Shen, S. T. Nguyen, and L. C. Brinson.Graphitic nanofillers in pmmananocomposites--an investigation of particle size and

dispersion and their influence on nanocomposite properties.*Journal of Polymer Science Part B: Polymer Physics*, 45(15):2097–2112, 2007.

[9] Gorga, R.E. and Cohen, R.E. (2004). Toughness Enhancements in Poly(methyl methacrylate) byAddition of Oriented Multiwall Carbon Nanotube,J. Polym. Sci., Part B: Polym. Phys.,42(14):2690–2702.

[10] WengeZheng and Shing-Chung Wong.Electrical conductivity and dielectric properties of pmma/expanded graphite composites.*Composites Science and Technology*, 63(2):225 – 235, 2003.

[11] Suprakas Sinha Ray and Masami Okamoto. Polymer/layered silicate nanocomposites: a review from preparation to processing. *Progress in Polymer Science*, 28(11):1539 – 1641, 2003.

[12] Bharadwaj RK. Modeling the barrier properties of polymerlayered silicate nanocomposites. Macromolecules 2001;34:1989–92.

[13] Hans M.L. and Lowman A.M. Biodegradable nanoparticles for drug delivery and targeting. *Current Opinion in Solid State & Materials Science*, 6(4):319–327, 2002.

[14] Spanhel, L., and Anderson, M.A., Semiconductor clusters in the Sol-gel Process: Quantized Aggregation, Gelation, and Crystal Growth in Concentrated ZnO Colloids, *J. Am. Chem. Soc.* 113, 2826-2833,(1991).

[15] Oner, M., Norwig, J., Meyer, W.H., and Wegner, G., Control of ZnO Crystallization by a PEO-b-PMAA Diblock Copolymer, *Chem. Mater.* 10, 460-463,(1998).

[16] Oliveira, A. P. A., Hochepied, J-F., Grillon, F., and Berger, M.H., Controlled

Precipitation of Zinc Oxide Particles at Room Temperature, *Chem. Mater.* 15, 3202-

3207,(2003).

[17] Demir, M. M., Munoz-Espi, R., Lieberwirth, I., and Wegner, G., Precipitation of monodisperse ZnO nanocrystals via acid-catalyzed esterification of zinc acetate, *J. Mater. Chem.* 16, 2940-2947,(2006).

[18] Rubinstein, M. and Colby, R. H., Polymer Physics, 2003, England: Oxford.

[19]DiNoia, T. P., Park, I. H., McHugh, M. A., van Zanten, J. H.,Obervation ofPolymer Chain Contraction near the Overlap Concentration, *Macromolecules*, 38, 9393-9395, (2005).

[20] Hiemenz, P. C., Polymer Chemistry, 1984, United States of America: Marcel Dekker Inc.

[21] Knappe, P., Bienert, R., Weidner, S., Thünemann, A. F., Characterization of poly(N-vinyl-2-pyrolidone)s with broad size distrivutions, *Polymer* , 51,1723-1727, (2010).

[22] Sartor, Marta. "Dynamic Light Scattering" University of California – San Diego.http://physics.ucsd.edu/neurophysics/courses/physics_173_273/dynamic_light_scattering_03.pdf

[23] Fixman, M., Radius of Gyration of Polymer Chains, *J. Chem. Phys*. **36**, 306 (1962)

[24] Rubinstein, M. and Colby, R. H., Polymer Physics, 2003, England: Oxford University Press

[25] Kokhlov, A. R., Les Houches, Lecture 6, Light Scattering in Polymer Solutions.

[26] Kokhanovsky, A. A., Light Scattering Reviews, 2013, Germany: Springer Berlin Heidelberg

[27] Netz, R. and Andelman, D., Neutral and charged polymers at interfaces, *Phys. Rep.* 380, 1-95,(2003).

[28] Bera, A., Basak, D., Effect of Surface Capping withPoly(vinyl alcohol) on the Photocarrier Relaxation of ZnO Nanowire. *Appl. Mater. Inter,* 1(9), 2066-2070, 2009.

[29] Hamad, I.; Al-Hanbali, O.; Hunter, A. C.; Rutt, K. J.; Andresen, T. L.; Moghimi, S. M., Distinct Polymer Architecture Mediates Switching of Complement Activation Pathways at the Nanosphere-Serum Interface: Implications for Stealth Nanoparticle Engineering. *ACS Nano* **2010**, *4*, 6629-6638.

[30] Dutta, N.; Green, D., Nanoparticle Stability in Semidilute and Concentrated Polymer Solutions. *Langmuir***2008**, *24*, 5260-5269.

[31] Lupitskyy, R.; Motornov, M.; Minko, S., S, Single Nanoparticle Plasmonic Devices by the "Grafting to" Method. *Langmuir* **2008**, *24*, 8976-8980.

[32] Tjong, S. C., Structural and Mechanical Properties of Polymer Nanocomposites. *Mater Sci Eng.***2006**, *53*, 73-197.

[33] Balazs, A. C.; Emrick T.; Russell T. P., Nanoparticle Polymer Composites: Where Two Small Worlds Meet. *Science* **2006**,*134*, 1107-1110.

[34] Liu, J.; Gao, Y.; Cao, D.; Zhang, L.; Guo, Z., Nanoparticle Dispersion and Aggregation in Polymer Nanocomposites: Insights from Molecular Dynamics Simulation. *Langmuir* **2011**, *27*, 7926-7933.

[35] Gacitua, W. A.; Ballerini, A. ; Zhang, J., Polymer Nanocomposites: Synthesis and Natural Fillers A Review. *Clencia y tecnologia***2005**, *7*, 159-178.

[36] Ibbett, R. N., NMR Spectroscopy of Polymers. In Ibbett, R. N., Ed. Chapman and Hall: Glasgow, Scotland, 1993.

[37] van der Beek, G. P.; Cohen Stuart, M. A.; Cosgrove, T., Polymer Adsorption and Desorption Studies via ^{1}H-NMR Relaxation of the Solvent.*Langmuir* **1991**, *7*, 327-334.

[38] Scheutjens, J. M. H. M., Fleer, G. J., Statistical Theory of the Adsorption of Interacting Chain Molecules 2. Train, Loop and Tail Size Distribution, J. Phys. Chem, 84, 178-190, 1980.

[39] Mirau, P.A., A Practical Guide to Understandin the NMR of Polymers, 2005, United States of America: Wiley Inter-Science.

[40] Esumi, K.; Takamine, K.; Ono, M.; Osada, T.; Ichikawa, S., The Interaction of Poly(vinylpyrrolidone) and Solid Particles in Ethanol. *J.Colloid Interface Sci.* **1993**, *161*, 321-324.

[41] Macomber, R.S., A Complete Introduction to Modern NMR Spectroscopy, 1988, United States of America: Wiley Inter-Science.

[42] Magritek, L., Introductory NMR and MRI: Video 07: Measuring T_1 and T_2 Relaxation. In YouTube: 2009.

[43] Basic's of MRI, J.P. Hornak, 1996-2010, http://www.cis.rit.edu/htbooks/mri/chap-3/chap-3.htm, (Interactive Learning Software, Henietta, NY).

[44] Barnett, K. G.; Cosgrove, T.; Vincent, B.; Sissons, D. S.; Cohen Stuart, M. A., Measurement of the Polymer-Bound Fraction at the Solid-Liquid Interface by Pulsed Nuclear Magnetic Resonance. *Macromolecules* **1981**, *14*, (4), 1018-1020.

[45] Cosgrove, T.; Barnett, K. G., Driven Equilibrium Solid and Liquid Spin-Echo NMR Sequences. *J. Mag. Reson.* **1981**, *43*, 15-20

[46] Kuo-Feng, L.; Hsin-Ming C.; Hsu-Cheng H.; Li-Jiaun L.; Wen-Feng H., Band gap variation of size-controlled ZnO quantum dots synthesized by sol-gel method. *Chem. Phys. Lett.* **2005**, *409*, 208-211.

[47] Pesika, N. S.; Hu, Z.; Stebe, K. J.; Searson, P.C., Quenching of Growth of ZnO Nanoparticles by Adsorption of Octanethiol.*J. Phys. Chem.* **2002**, *106*, 6985-6990.

[48] Sesta, B.; Segre A. L.; D'Aprano A.; Proietti N., ^{1}H NMR, Surface Tension, Viscosity, and Volume Evidence of Micelle-Polymer Hydrophobic Interactions: LiPFN-PVP System. *J. Phys. Chem.* **1997***, 101,*198-204.

[49] SDBSWeb: http://riodb01.ibase.aist.go.jp/sdbs/ (National Institute of Advanced Industrial Science and Technology, accessed on December 3, 2012).

[50] Lipowsky, P.; Hedin, N.; Bill, J.; Hoffmann, R. C.; Ahniyaz, A.; Aldinger, F.; Bergstöm, L.; Controlling the Assembly of NanocrystallineZnO Films by a Transient Amorphous Phase in Solution, *J.Phys. Chem. C,***2008**, 112, 5373-5383.

[51] van Dijken, A.; Meulenkamp, E. A.; Vanmaekelbergh, D.; Meijerink, A.; The luminescence of nanocrystalline ZnO particles: the mechanism of the ultraviolet and visible emission, *J. Lumin*., **2000**, 87-89, 454-456.

[52] Guo, L.; Yang, S.; Synthesis and Characterization of Poly(vinylpyrolidone)- Modified Zinc Oxide Nanoparticles, *Chem. Matter.*, **2000**, 12, 2268-2274.

[53] Barnet, K. G.; Cosgrove, T.; Vincent, B.; Sissons D. S.; Measurement of the Polymer-Bound Fraction at the Solid-Liquid Interface by Pulsed Nuclear Magnetic Resonance. *Macromolecules.***1981**, 14, 1018-1020.